Global Biogeochemical Cycles

RESEARCH ARTICLE
10.1029/2018GB006101

Key Points:
- Phytoplankton long-term photoprotective response is mediated in most parts of the ocean by a variable pool of xanthophyll pigments
- The variability in the pool of xanthophyll pigments is mainly driven by changes in phytoplankton community composition in the tropical and subtropical ocean
- At high latitudes other photoprotection mechanisms play a role, and both taxonomic shifts and photoacclimation determine community pigment signature

Supporting Information:
- Supporting Information S1

Correspondence to:
E. Álvarez,
eva.alvarez@awi.de

Citation:
Álvarez, E., Thoms, S., Bracher, A., Liu, Y., & Völker, C. (2019). Modeling photoprotection at global scale: The relative role of nonphotosynthetic pigments, physiological state, and species composition. *Global Biogeochemical Cycles*, *33*. https://doi.org/10.1029/2018GB006101

Received 6 OCT 2018
Accepted 16 JUN 2019
Accepted article online 22 JUN 2019

©2019. American Geophysical Union. All Rights Reserved.

Modeling Photoprotection at Global Scale: The Relative Role of Nonphotosynthetic Pigments, Physiological State, and Species Composition

E. Álvarez[1], S. Thoms[1], A. Bracher[1,2], Y. Liu[1,3], and C. Völker[1]

[1]Alfred Wegener Institute Helmholtz Centre for Polar and Marine Research, Bremerhaven, Germany, [2]Institute of Environmental Physics, University of Bremen, Bremen, Germany, [3]Faculty of Biology and Chemistry, University of Bremen, Bremen, Germany

Abstract Microalgae are capable of acclimating to dynamic light environments, as they have developed mechanisms to optimize light harvesting and photosynthetic electron transport. When absorption of light exceeds photosynthetic capacity, various physiological protective mechanisms prevent damage of the photosynthetic apparatus. Xanthophyll pigments provide one of the most important photoprotective mechanisms to dissipate the excess light energy and prevent photoinhibition. In this study, we coupled a mechanistic model for phytoplankton photoinhibition with the global biogeochemical model Regulated Ecosystem Model version 2. The assumption that photoinhibition is small in phytoplankton communities acclimated to ambient light allowed us to predict the photoprotective needs of phytoplankton. When comparing the predicted photoprotective needs to observations of pigment content determined by high-performance liquid chromatography, our results showed that photoprotective response seems to be mediated in most parts of the ocean by a variable ratio of xanthophyll pigments to chlorophyll. The variability in the ratio appeared to be mainly driven by changes in phytoplankton community composition. Exceptions appeared at high latitudes where other energy dissipating mechanisms seem to play a role in photoprotection and both taxonomic changes and physiological acclimation determine community pigment signature. Understanding the variability of community pigment signature is crucial for modeling the coupling of light absorption to carbon fixation in the ocean. Insights about how much of this variability is attributable to changes in community composition may allow us to improve the match between remotely sensed optical data and the underlying phytoplankton community.

1. Introduction

Since phytoplankton organisms are living in a spatially and temporally dynamic light field, their cells have developed a variety of intracellular mechanisms to optimize light harvesting and utilization. Light fluctuations can be harmful to the photosynthetic machinery of microalgae when the harvesting of light energy exceeds photosynthetic carbon fixation capacity (Dubinsky & Schofield, 2010). Thus, to prevent damage of the photosynthetic apparatus caused by rapid light fluctuations, algal cells have evolved various physiological protective mechanisms for stress mitigation. These mechanisms are summarized under the term nonphotochemical quenching (NPQ; Lavaud, 2007). NPQ includes mechanistically distinct processes with likely independent evolutionary origins (Magdaong & Blankenship, 2018), but they share the nonradiative dissipation of excess energy within the photosynthetic apparatus as a common purpose.

Xanthophyll pigments (oxygenated carotenoids) are involved either directly or indirectly in the NPQ of excess light energy in the antenna of photosystem II complexes (PSII). They are ubiquitous in the global ocean (Bricaud et al., 2004; Demmig-Adams & Adams, 1996; Trees et al., 2000). In eukaryotes, one of the main mechanisms that xanthophylls use to perform their photoprotective function is the so-called xanthophyll cycle (XC; Lavaud, 2007). This mechanism involves the light-regulated switching of PSII from a light-harvesting state to an energy dissipating state (Brunet et al., 2011). But also, photosynthetic organisms that do not possess an active XC, such as cyanobacteria, possess xanthophylls with central functions in energy dissipation (Wilson et al., 2006) and locate some carotenoids in the cytoplasmic membrane for protection from high light (Masamoto et al., 1999). The role of xanthophylls is crucial in the modulation of the high light response via the kinetics and amplitude of NPQ that helps to protect the photosynthetic centers against the destructive influence of harmful radiation (Müller et al., 2001).

The amount of xanthophyll pigments relative to total chlorophyll (Chla) is a distinctive feature of different phytoplankton types. It reflects the selective pressure on variable pigment composition in local phytoplankton communities adapted to varying environmental conditions. Accessory pigments have been used as general diagnostic markers for specific phytoplankton groups, and changes in the community pigment ratios can be used to derive changes in taxonomic composition (Mackey et al., 1996). However, the ratios of individual accessory pigments to Chla can also vary as a function of physiological state. The plasticity in the response of phytoplankton to irradiance is species specific (MacIntyre et al., 2002). This plasticity depends on the photoacclimation ability and light history of the phytoplankton cells (Moore et al., 2006) and on the species-specific efficiency of the photoregulative mechanisms (Goss & Jakob, 2010; Lavaud, 2007). Whereas photoregulation involves fast photoprotective reactions that occur on a shorter time scale than pigment synthesis responses, photoacclimation includes longer-term mechanisms of photoresponse that involve changes in pigment content and composition (Demers et al., 1991). Ultimately, photoresponse is determined by the interaction between fast photoregulation and longer-term photoacclimation (Brunet & Lavaud, 2010) in the framework of a given genetic background.

Under acclimation to a prolonged light regime, from hours to seasons, phytoplankton cells change the size of the light harvesting apparatus to saturate dark reactions or to protect PSII. This means typically that the cellular content of photosynthetic pigments tends to increase under low light and to decrease under high light. Photoacclimation to low light includes not only chlorophyll (Chla) but also the accumulation of other photosynthetic accessory pigments, such as fucoxanthin in diatoms or peridinin in dinoflagellates that ensure an efficient utilization of the available light by absorbing photons outside the range of wavelengths accessible to Chla molecules. Photoprotective xanthophyll pigments accumulate in high-light-exposed cells that show higher xanthophyll content relative to Chla (MacIntyre et al., 2002). The ratios of photoprotective pigments to Chla concentrations can be used as quantitative markers for photophysiological state (Stolte et al., 2000). The variations in the pool size of xanthophyll pigments can provide information on the "average" light climate to which the cells have been exposed in the past hours/days.

Xanthophylls participate in the fast photoregulative reactions. Despite differences in their particular mechanisms of action (Fujiki & Taguchi, 2001; Horton et al., 2000; Jahns et al., 2009; Ting & Owens, 1993), it is clear that the function of the XC takes place in time scales of seconds to minutes and allows algae to accommodate to rapid changes in the light field without net change in pigments content. XC is activated when the incident light becomes excessive with respect to the optimum, which is necessary to maximize photosynthesis (Dubinsky & Stambler, 2009). Two different XCs have been described for eukaryotic algae. In the violaxanthin cycle, violaxanthin is reversibly converted into zeaxanthin by fast de-epoxidation using the intermediate antheraxanthin. The diadinoxanthin-diatoxanthin cycle involves the reversible conversion of diadinoxanthin into diatoxanthin. Violaxanthin cycle is active in all land plants, brown algae, and most of the green algae; diadinoxanthin-diatoxanthin cycle is active in a wide range of different algae including diatoms and haptophytes (for reviews see Goss & Jakob, 2010; Jahns et al., 2009). Since the time scale of xanthophyll cycling is much shorter than that of photoacclimation, both epoxidated and de-epoxidated xanthophylls act as photoprotection in the medium to long term and contribute to the photoprotection ability of phytoplankton communities.

Description of photoacclimation via the changes in Chla content is by now virtually standard in ocean biogeochemical models, mostly in terms of the parameterization given by Geider et al. (1998) and sometimes also by Geider et al. (1997). Despite the relevant role of xanthophylls in algae and its possibly important implications, less emphasis has been placed on the capacity of different phytoplankton species or groups to acclimate or regulate photophysiology through photoprotective pigments (Brunet & Lavaud, 2010). There are only a few models that explicitly represent the dynamics of reaction centers and the xanthophyll-mediated photoprotection. Polimene et al. (2012) proposed a model of DD and DT production through conversion of other pigments and de novo synthesis and hence predict the long-term photoprotective response in Bacilliarophyta and Haptophyta. Gustafsson et al. (2014) proposed a model that describes xanthophyll synthesis and cycling in zooxanthella and hence predicts the short-term oxidative stress that leads to coral bleaching. In both cases, the focus on a specific pigment type or mechanism of action permitted the authors to gain insight into particular situations, such as coastal areas dominated by diatoms (Polimene et al., 2014) or corals reefs of the Great Barrier Reef (Baird et al., 2018). Pigment- or mechanism-dependent models are challenging to extrapolate to diverse phytoplankton communities.

Models that do not parameterize short-term photoprotective mechanisms have the advantage that they can be generalized to diverse phytoplankton communities across the global ocean (Han, 2002; Han et al., 2000; Marshall et al., 2000; Ross et al., 2011; Zonneveld, 1998). These models predict the role of NPQ influencing the activity of PSII and consider the role of photoprotective pigments only implicitly. The mechanistic model of photoinhibition proposed by Marshall et al. (2000) accounts for changes in Chla-specific absorption cross-section and quantum yield of photosynthesis driven by the relative amount of active PSII. The decrease in both variables under high light conditions leads to the photoinhibition of the light harvesting apparatus and therefore to the decrease in photosynthetic rate. The fraction of PSII available for photochemistry depends on the protective effect of NPQ involving both closed reaction centers and photoprotective pigments. Rather than assuming any particular short-term mechanism of action for these latter, a variable xanthophyll pool size simulates the resilience of the phytoplankton community to photodamage.

In this study we used the Marshall model as a tool to evaluate the relevance of the different components of NPQ in the global ocean. Avoiding the representation of the full details of the species-specific short-term photoprotective mechanisms allowed us to represent long-term photoprotection in a global diverse ecosystem. We implemented both the phytoplankton growth models of Geider et al. (1998) and Marshall et al. (2000) into the Regulated Ecosystem model version 2 (REcoM2; Hohn, 2009; Schartau et al., 2007). Thereby, we present an ecosystem model that represents phytoplankton diversity with two phytoplankton groups that have group-specific photoprotective needs. Our approach was based on the major assumption that the photoinhibition predicted by the Marshall model should be negligible in phytoplankton communities fully acclimated to ambient light. The difference between the photosynthesis-irradiance curves predicted with and without photoinhibition, that is, by the Marshall and Geider models, respectively, can be considered a measure of the need for photoprotection in order to minimize such photoinhibition. We hypothesize that these photoprotection needs are covered mostly by a variable pool of photoprotective xanthophylls. By comparing the predicted photoprotection needs with global field observations of photoprotective carotenoid content, we evaluated the relevance of nonphotosynthetic xanthophylls for the photoprotection of the phytoplankton community at a global scale. Finally, we explored whether changes in the community aggregated xanthophyll pool were driven by intragroup physiological acclimation and/or by changes in community composition.

2. Model

2.1. Phytoplankton Bio-Optical Model

Within the mechanistic model of photoinhibition by Marshall et al. (2000), the Marshall model, the light harvesting apparatus is divided into two states, PSII with a functional D1 protein and hence active for light harvesting and PSII whose D1 protein has been damaged and hence can no longer participate in photosynthetic electron transfer. The relative amounts of these two types of PSII are represented by the state variables AD1 and DD1, which represent the relative amount of active and damaged PSII, respectively. Definitions of the variables and their units are summarized in Table 1. The model consists of two parts: The first part describes the damage-repair cycle, a set of functions that define the rates of damage to the D1 proteins of the PSII and the rate at which those damaged proteins are repaired; the second part predicts photoinhibition based on the statement that the amount of AD1 at a given time influences the light harvesting ability of the cell and hence the initial slope of the photosynthesis versus light curve ($P^C{}_{\mathrm{phot}}$–E). Since the original paper by Marshall et al. (2000) contains some equations that do not balance, we included some modifications to reproduce the model behavior shown in the original publication (equations (1) to (7) in Table 2). For a detailed analysis of the modifications made to Marshall et al. (2000), see the supporting information (Flynn et al., 1999; Flynn & Flynn, 1998).

2.1.1. Damage and Repair of D1 Proteins

The rate of damage to AD1 (Gd) is modeled as a linear function of photon dose (equation 1). The slope of the relationship represents the target size for photodamage to PSII (square meter per Joule). The two NPQ mechanisms that prevent damage to AD1 are (i) the quenching provided by already damaged reaction centers (qRC) that protects the cell from further damage via multiplication with the term (1 − DD1) and (ii) the antenna-based NPQ (Q_e) that decreases Gd via multiplication with the term ($1 - Q_e$). Whereas qRC is proportional to DD1 that is a state variable in the model, Q_e is not related to any explicit representation of

Table 1
Definitions of State, Intermediate, and Input Variables in the Phytoplankton Growth model

Variable	Definition	Units
State variables		
C	Carbon	mmolC m^{-3}
N	Nitrogen	mmolN m^{-3}
Si	Silica	mmolSi m^{-3}
Chla	Photosynthetic pigments	mgChla m^{-3}
AD1	Functioning D1 relative to total D1	Dimensionless
DD1	Damaged D1 relative to total D1	Dimensionless
Intermediate variables		
Gd	Damage rate	d^{-1}
Rep	Repair rate	d^{-1}
ϕ	Quantum yield of photosynthesis	mmolC J^{-1}
Q_e	Antenna-based non photochemical quenching	Dimensionless
a^*_{NP}	Cellular absorption cross section	m^2 mgChla^{-1}
α_{NP}	Initial slope of the photosynthesis light curve of damaged cells	m^2 molC gChla^{-1} J^{-1}
Q	Nitrogen to carbon quota	mol mol^{-1}
Q_{Si}	Silica to carbon quota	mol mol^{-1}
Θ	Chla to carbon quota	g mol^{-1}
$LimQ_{min}$	Limitation term by approach to Q_{min}	Dimensionless
$LimQ^{Si}{}_{min}$	Limitation term by approach to $Q^{si}{}_{min}$	Dimensionless
Nlimit	Nutrient growth-limitation term	Dimensionless
$LimQ_{max}$	limitation term by approach to Q_{max}	Dimensionless
$LimQ^{Si}{}_{max}$	Limitation term by approach to $Q^{si}{}_{max}$	Dimensionless
Tfunc	Arrhenius function	Dimensionless
$P^C{}_{phot}$	Rate of photosynthesis	d^{-1}
$P^C{}_{max}$	Maximum rate of photosynthesis	d^{-1}
R	Phytoplankton respiration	d^{-1}
RChl	Loss rate of Chla	d^{-1}
$V^C{}_N$	Nitrogen uptake	molN molC^{-1} d^{-1}
$V^N{}_{max}$	Maximum nitrogen uptake	molN molC^{-1} d^{-1}
$V^C{}_{Si}$	Silica uptake	molSi molC^{-1} d^{-1}
$V^{Si}{}_{max}$	Maximum silica uptake	molSi molC^{-1} d^{-1}
Input variables		
T	Temperature	°K
E	Irradiance	J $m^{-2}d^{-1}$
Ni	Dissolved inorganic nitrogen (DIN)	mM
dSi	Dissolved silica	mM
Fe	Dissolved iron	μM

nonphotosynthetic pigments. In the original formulation Q_e is modified by a correction factor (*Ds*) that is intended to reflect the differential resilience of different species to photodamage via xanthophyll-based NPQ. By setting the parameter *Ds* to a constant value of 1, the Marshall model assumes a constant xanthophyll pigment pool size.

The repair rate of D1 proteins (*Rep*) is modeled as a function of DD1, the relative amount of damaged PSII that are ready to be repaired. Repair of DD1 consists on several steps. The apparent bottleneck of the whole process is the enzymatic removal of damaged proteins (Mellis, 1999). Hence, *Rep* must reach a maximum and has the form of a Michaelis-Menten function where *Y* is the maximum repair rate and *Z* the half saturation constant (equation (2)). As repair requires de novo synthesis of D1 proteins, *Rep* is limited by nutrient availability (*Nlimit*) in the original formulation (Marshall et al., 2000). We included a temperature dependency (*Tfunc*) given the temperature restrictions on D1-protein turnover (Ni et al., 2017). The change in AD1 is set to the difference between the damage and repair rates to D1 proteins (equation (3)) and the amount of DD1 is equal to 1−AD1 (equation (4)).

2.1.2. Effect of AD1 and NPQ on α

The photochemical efficiency of PSII (ϕ), defined as carbon fixed per unit of light absorbed, depends on the fraction of AD1 proteins available to photochemistry. The closure of reaction centers leads to a decrease in the value of ϕ. However, a loss of active photosystems of up to 25% has been found to have no impact on ϕ

Table 2
Phytoplankton Growth Model Equations

Eq.	Equations	Source
1	$Gd = (X \times E) \times AD1 \times (1 - Q_e)$	Modified from (Marshall et al., 2000)
2	$Rep = \left(\frac{Y \times DD1}{Z + DD1}\right) \times Nlimit \times Tfunc$	(Marshall et al., 2000)
3	$\frac{dAD1}{dt} = DD1 \times Rep - AD1 \times Gd$	Modified from (Marshall et al., 2000)
4	$\frac{dDD1}{dt} = AD1 \times Gd - DD1 \times Rep$	Modified from (Marshall et al., 2000)
5	$\phi = \min\left(\frac{\phi_{max}}{F} \times AD1, \phi_{max}\right)$	Modified from (Marshall et al., 2000)
6	$Q_e = 1 - {}^{\phi}/_{\phi_{max}}$	Modified from (Marshall et al., 2000)
7	$\alpha_{NP} = a^*_{NP} \times \phi \; ; \; a^*_{NP} = a^*_{PH} \times (1 - Q_e)$	(Marshall et al., 2000)
8	$LimQ_{min} = 1 - e^{-50 \times (abs(Q_{min} - Q) - (Q_{min} - Q))^2}$	(Hohn, 2009)
9	$LimQ^{Si}_{min} = 1 - e^{-1000 \times \left(abs\left(Q^{Si}_{min} - Q_{Si}\right) - \left(Q^{Si}_{min} - Q_{Si}\right)\right)^2}$	(Hohn, 2009)
10	$Nlimit_d = \min\left(LimQ_{min}, LimQ^{Si}_{min}, \frac{Fe}{Fe + k_{Fe}}\right); Nlimit_{nd} = \min\left(LimQ_{min}, \frac{Fe}{Fe + k_{Fe}}\right)$	Liebig's law
11	$LimQ_{max} = 1 - e^{-1000 \times (abs(Q - Q_{max}) - (Q - Q_{max}))^2}$	(Schartau et al., 2007)
12	$LimQ^{Si}_{max} = 1 - e^{-1000 \times \left(abs\left(Q_{Si} - Q^{Si}_{max}\right) - \left(Q_{Si} - Q^{Si}_{max}\right)\right)^2}$	(Hohn, 2009)
13	$Tfunc = e^{-Ae \times \left(\frac{1}{T} - \frac{1}{T_{ref}}\right)}$	(Geider et al., 1998)
14	$P^C_{phot} = P^C_{max} \times \left(1 - e^{-\alpha\theta E / {}_{P}max^{C}}\right) \; ; \; P^C_{max} = P^C_{ref} \times Nlimit \times Tfunc$	(Webb et al., 1974)
15	$R = R_{ref} \times LimQ_{max} + \zeta \times V^C_N + \vartheta \times V^C_{Si}$	(Geider et al., 1998)
16	$\frac{dC}{dt} = C \times \left(P^C_{phot} - R - \eta_C \times LimQ_{max}\right)$	(Geider et al., 1998)
17	$\frac{dChla}{dt} = Chla \times \left(\frac{V^C_N \times Q^{Chl}_N}{\theta} \times \frac{P^C_{phot}}{\alpha \times \theta \times E} - RChl\right)$	(Geider et al., 1998)
18	$RChl = k \times \left(1 - e^{-\alpha\theta E / P^C_{max}}\right)$	(Álvarez et al., 2018)
19	$V^C_N = V^N_{max} \times \frac{Ni}{(Ni + k_N)} \; ; \; V^N_{max} = V^C_{ref} \times P^C_{max} \times Q_{max} \times LimQ_{max}$	(Geider et al., 1998)
20	$\frac{dN}{dt} = C \times V^C_N - N \times \eta_N \times LimQ_{max}$	(Geider et al., 1998)
21	$V^C_{Si} = V^{Si}_{max} \times \frac{dSi}{(dSi + k_{Si})} \; ; \; V^{Si}_{max} = V^C_{ref} \times P^C_{ref} \times Tfunc \times Q^{Si}_{max} \times LimQ_{max} \times LimQ^{Si}_{max}$	(Hohn, 2009)
22	$\frac{dSi}{dt} = C \times V^C_{Si} - Si \times \eta_{NSi} \times LimQ_{max}$	(Hohn, 2009)

Note. Details on the modifications made to Marshall et al. (2000) model in the Supporting Information (Flynn et al., 1999; Flynn & Flynn, 1998).

(Park et al., 1995). So for AD1 larger than 0.75, ϕ equals ϕ_{max}, and for AD1 smaller than 0.75, ϕ decreases linearly with D1 (equation (5)). The slope is set to $\phi_{max}/0.75$, so ϕ varies from ϕ_{max} to 0.

The buildup of a proton gradient across the thylakoid triggers the de-epoxidation of xanthophylls (Goss & Jakob, 2010) and hence an increase in Q_e. Since pH is not explicitly taken into account in the Marshall model, the latter assumes that ϕ is correlated with pH and uses ϕ as a proxy for Q_e (equation (6)). The slope $1/\phi_{max}$ makes Q_e a relative quantity that varies between 0 and 1.

Q_e has two roles in the model. It decreases the damage rate to D1 proteins (equation (1)) and decreases the Chla-specific optical absorption cross-section of photosynthetic pigments (a^*_{NP}) (equation (7)). Although

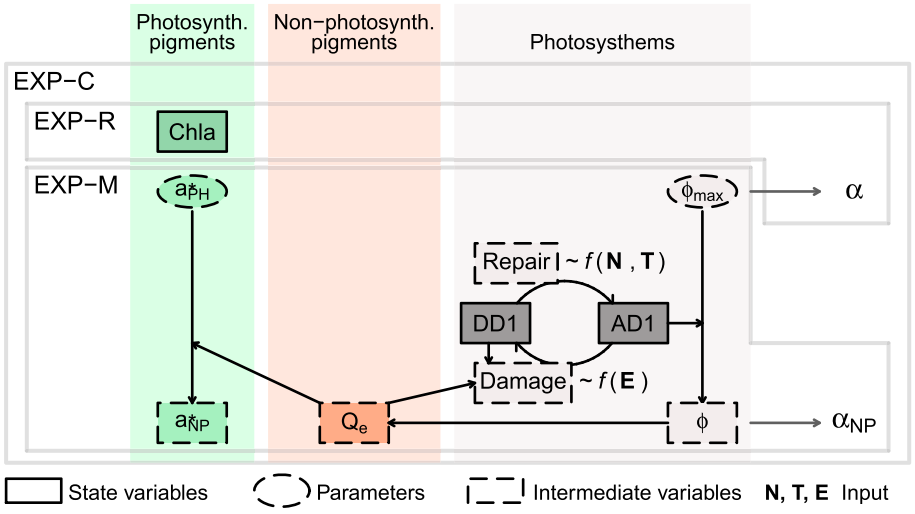

Figure 1. Schematic showing the parts of the model used in each experiment. The model is divided into photosynthetic and nonphotosynthetic pigments and reaction center dynamics. State, intermediate, input variables, and parameters are distinguished.

the latter is the simplest description of the effects of Q_e on a^*_{NP}, it is sufficient to represent the decrease in a^*_{NP} as observed from saturating to inhibitory light levels (Kolber et al., 1988).

The decrease in the absorption cross-section acts alongside ϕ decrease to decrease the initial slope of the P^C_{phot}–E curve (α_{NP}). α_{NP} is generally described as the light limited slope of the P^C_{phot}–E curve since under light saturated conditions the photosynthesis is limited by dark reactions. However, the net result of the Marshall model is making α_{NP} variable along the curve. The decrease in α_{NP} under high light conditions reverts the limit for photosynthesis from dark to light reactions, which eventually leads to photoinhibition.

2.1.3. Combining the Models by Marshall and Geider et al. (1998)

The dynamic phytoplankton growth model by Geider et al. (1998) sets the initial slope of the P^C_{phot}–E curve (α) as a constant parameter. With α being constant along the whole P^C_{phot}–E curve and with no other photoinhibitory parameter being considered, photoinhibition does not take place. The differences between Geider and Marshall approximations are summarized in Figure 1. If we assume that photoinhibition is negligible in phytoplankton communities acclimated to ambient light (Cullen et al., 1992), the difference between the P^C_{phot}–E curves with (Marshall) and without photoinhibition (Geider) reflects the need for photoprotection in order to limit such photoinhibition. The difference between Geider and Marshall P^C_{phot}–E curves is given by the difference between α and α_{NP}. Hence, the difference between α and α_{NP} reflects a photoprotection gap that could be filled by the missing elements in the description of NPQ, such a variable pool of nonphotosynthetic pigments but also by any other mechanism not described explicitly such as constitutive heat dissipation. By comparing the predicted photoprotection gap to observations of photoprotective carotenoids under natural conditions, we tested whether the gap is filled by the presence of nonphotosynthetic pigments, or if further mechanisms are necessary to complete photoprotection.

We performed three experiments with different settings for our model:

EXP-R equivalent to the dynamic phytoplankton model by Geider, only α was computed and used in the P^C_{phot}–E curve for production.

EXP-M equivalent to the original Marshall model, only α_{NP} was computed and used in the P^C_{phot}–E curve for production.

EXP-C both α and α_{NP} were computed, α was used in the P^C_{phot}–E curve for production, and the difference between α and α_{NP} was explored to evaluate photoprotection requirements.

2.2. Implementation Into REcoM2

The variability in pigment composition in a diverse phytoplankton community is not only dependent on the direct effect of environmental conditions on light harvesting traits for a particular phytoplankton group.

Table 3
Definitions of Parameters With Values for the Two Phytoplankton Groups

Parameter	Definition	Value diatoms	Value nondiatoms	Units
α	Initial slope of the photosynthesis irradiance curve	0.19	0.14	m^2 molC $gChla^{-1}$ J^{-1}
φ_{max}	Maximum quantum yield	$3.1{\cdot}10^{-4}$	$2.3{\cdot}10^{-4}$	mmolC J^{-1}
a^*_{PH}	Chlorophyll absorption cross section	0.007	0.007	m^2 $mgChla^{-1}$
F	Minimum AD1 to keep $\varphi=\varphi_{max}$	0.75	0.75	relative (0-1)
X	Target size for photoinactivation	$1.5{\cdot}10^{-7}$	$7.5{\cdot}10^{-7}$	m^2 J^{-1}
Y	Maximum repair rate	10	10	d^{-1}
Z	Half saturation constant repair	0.3	0.3	relative (0-1)
P^C_{ref}	Maximum rate of photosynthesis	3.5	3	d^{-1}
R_{ref}	Maintenance respiration rate	0.01	0.01	d^{-1}
V^C_{ref}	Maximum nitrogen uptake	0.7	0.7	molN $molC^{-1}$ d^{-1}
k_N	Half-saturation constant nitrate uptake	1	0.55	mmolN m^{-3}
k_{Si}	Half-saturation constant silica uptake	4	—	mmolSi m^{-3}
k_{Fe}	Half-saturation constant iron uptake	0.12	0.02	µmolFe m^{-3}
Q_{min}	Minimum cell quota of nitrogen	0.04	0.04	molN $molC^{-1}$
Q_{max}	Maximum cell quota of nitrogen	0.2	0.2	molN $molC^{-1}$
Q^{Si}_{min}	Minimum cell quota of silica	0.04	—	molSi $molC^{-1}$
Q^{Si}_{max}	Maximum cell quota of silica	0.2	—	molSi $molC^{-1}$
Q^{Chl}_N	Maximum Chla to nitrogen ratio	4.2	3.78	gChl $molN^{-1}$
Q^{SI}_N	Minimum silica to nitrogen ratio	0.3	—	molSi $molN^{-1}$
ζ	Cost of N biosynthesis	2.33	2.33	molC $molN^{-1}$
?	Cost of Si biosynthesis	0	—	molC $molSi^{-1}$
k	Maximum loss rate of Chla	0.25	0.15	d^{-1}
η_C	Phytoplankton loss of C	0.1	0.1	d^{-1}
η_N	Phytoplankton loss of N	0.05	0.05	d^{-1}
η_{Si}	Phytoplankton loss of Si	0.05	—	d^{-1}
T_{ref}	Reference temperature	288.15		°K
Ae	Linear slope Arrhenius function	4500		°K
κ_W	Total light attenuation due to water	0.04		m^{-1}
a_{CHL}	Chla-specific attenuation coefficient	0.03		m^2 mg $Chla^{-1}$

Community composition influences the community aggregated pigment signatures. We chose the RecoM2, which provides the simplest framework to include phytoplankton diversity since it describes the dynamics of two phytoplankton groups with a detailed description of their elemental composition. The rest of the ecosystem is completed with zooplankton, detritus, and main nutrients compartments. Ocean circulation and mixing is derived from the MIT general circulation model. Details about the complete model setup can be consulted in the appendix to Hauck et al. (2013).

2.2.1. Phytoplankton Diversity

RecoM2 describes the dynamics of two phytoplankton types, diatoms and nondiatoms. The difference between groups is merely functional, as diatoms require silica and other phytoplankton do not. However, differences in parameter values between the two groups (Table 3) are size related, and the diatom group can be ascribable to large-sized phytoplankton while other phytoplankton represents smaller phytoplankton. We kept α values larger for diatoms compared to the values for small phytoplankton. This have provided realistic distribution of primary production in previous applications of REcoM2 (Álvarez et al., 2018; Schourup-Kristensen et al., 2014). With all PSII being active for photochemistry, α_{NP} should equal α. Since the Marshall model splits α_{NP} into absorption (a^*_{NP}) and photochemical (ϕ) components, we set the maximum values for those, a^*_{PH} and ϕ_{max}, in order to match the group specific α's (Table 3).

Literature values given for a^*_{PH} range from 0.005 to 0.025 $m^2{\cdot}mg{\cdot}Chla^{-1}$ (Kromkamp et al., 2001; Megard et al., 1979; Oliver & Ganf, 1988) and given the package effect on pigment concentrations, larger cells tend to have smaller values of a^*_{PH} (Bricaud et al., 2004). However, we kept a^*_{PH} equal for the two groups in 0.007 $m^2{\cdot}mg{\cdot}Chla^{-1}$, and hence, we have not considered a packaging effect. The light attenuation by phytoplankton (a_{CHL}) was also set constantly to 0.03 $m^2{\cdot}mg{\cdot}Chla^{-1}$ (Table 3). Experimental values given for ϕ_{max} range from $2.1{\cdot}10^{-5}$ to $4.8{\cdot}10^{-4}$ mmolC/J (Du et al., 2018; Kiefer & Mitchell, 1983; MacIntyre et al., 2002; Raven &

Crawfurd, 2012). In the field, higher ϕ_{max} have been documented in communities dominated by diatoms (Babin et al., 1996). So we gave ϕ_{max} of $3.1{\cdot}10^{-4}$ mmolC/J to diatoms (which generated an α of 0.19; Table 3) and $2.3{\cdot}10^{-4}$ mmolC/J to other phytoplankton (which generated an α of 0.14; Table 3). There were also group differences regarding the damage-repair cycle. Picoplankton are generally reported to have damage coefficients that are higher (Nagy et al., 1995; Six et al., 2007) than for green algae (Oliver et al., 2003; Serôdio et al., 2017), but not very different from the values in diatoms (Campbell & Tyystjärvi, 2012; Lavaud et al., 2016). In this work we assigned smaller damage coefficients to diatoms than to other phytoplankton and kept equal repair parameters (Table 3).

2.2.2. Phytoplankton Growth Model

The remaining part of the phytoplankton growth model was the same for the three experiments described above and included the dynamics of the elemental pools of carbon (C), photosynthetic pigments (Chla), nitrogen (N), and silica (Si; equations (8) to (22) in Table 2). The nutrient limitation terms in REcoM2 include $LimQ_{min}$ and $LimQ^{Si}{}_{min}$ that limit processes dependent on the content of proteins for enzymatic reactions and thus decrease when protein content approaches the minimum cellular quota (equations (8) and (9)). *Nlimit* (equation (10)) is a combined nutrient-limitation term that computes the minimum of $LimQ_{min}$, $LimQ^{Si}{}_{min}$, and a limitation term for Fe in Michaelis-Menten form for diatoms ($Nlimit_d$) and only the minimum of $LimQ_{min}$ and the term for Fe for other phytoplankton ($Nlimit_{nd}$). $LimQ_{max}$ and $LimQ^{Si}{}_{max}$ limit processes that saturate when protein content approaches the maximum cellular quota (equations (11) and (12)). The temperature dependency is an Arrhenius function (Geider et al., 1998; equation (13)). All limitation terms multiply the rates they regulate, and hence, they are 1 for no limitation and approach 0 as limitation increases.

The $P^C{}_{phot}$–E curve is used as the exponential formulation in Geider et al. (1998) where maximum photosynthesis rate ($P^C{}_{max}$) is limited by *Nlimit* and *Tfunc* (equation (14)). Phytoplankton respiration includes maintenance respiration and the cost of biosynthesis (equation (15)). The variation in C content is set to the rate of photosynthesis minus respiration and excretion (equation (16)).

The synthesis of photosynthetic pigments (represented by Chla) is equivalent to N assimilation regulated by the photochemical use of absorbed light, a term that allows photoacclimation (Geider et al., 1998; equation (17)). The loss of Chla is light dependent to account for photodamage in the light harvesting apparatus (Álvarez et al., 2018; equation (18)).

Although N and Si pools are not central in this work, they both shape the stoichiometric ratios that limit production and biosynthetic processes. N uptake ($V^C{}_N$) depends on available DIN, the half saturation constant k_N, and the maximal uptake rate ($V^C{}_{max}$) that is proportional to $P^C{}_{max}$ and declines when Q approaches Q_{max} (equation (19)). The rate of N assimilation is set to uptake minus excretion rates, and the latter is also limited by $LimQ_{max}$ (equation (20)). Si uptake ($V^C{}_{Si}$) (equation (21)) and assimilation (equation (22)) are formulated in an equivalent way to those of N (Hohn, 2009).

2.2.3. The Rest of the Ecosystem and the Global Circulation Model

REcoM2 completes the ecological module with one zooplankton and one detritus compartment, and inorganic and organic forms of the main nutrients. Temperature (T) and dissolved nutrients (DIN, dSi, and Fe), like all other biogeochemical model variables, are advected and mixed by the ocean circulation derived from the MIT general circulation model. Average light (E) is computed in depth layers as an exponential decreasing function of depth with a depth-dependent light attenuation coefficient with two components, the attenuation coefficient due to water (κ_W) and the attenuation due to phytoplankton, proportional to total Chla concentration ($a_{CHL} \times TChla$) (Table 3).

For our study, in each experiment REcoM2 was run in a nearly global model configuration from 80°S to 80°N on a horizontal 2° × 2° grid in the Northern Hemisphere and 2° × 2° times the cosine of the latitude in the Southern Hemisphere, with 30 depth layers (0 to 5,700 m). The model was initialized with the January climatological fields of temperature, salinity, nitrate, and silicate from the World Ocean Atlas 2009 (Antonov et al., 2010; Garcia et al., 2010; Locarnini et al., 2010) and with mean alkalinity and preindustrial CO_2 fields from the Global Ocean Data Analysis Project (GLODAP; Key et al., 2004). The initial field for dissolved Fe was obtained from PISCES output (Aumont et al., 2003), with values south of 45°S set to average Southern Ocean vertical profiles from Tagliabue et al. (2012), to avoid a high-iron bias there. The model was spun up for 4 years and analyzed for the next fifth year in a 10-daily temporal resolution.

Table 4
List of Data Sets With HPLC Measurements

Data set	Source
MAREDAT pigments	Peloquin et al. (2013)
ANT23.1 (PS69)	Bracher et al. (2015a, 2015b)
ANT24.1 (PS71.1)	Bracher (2015b, 2015e); Bracher et al. (2015b)
ANT24.4 (PS71.4)	Bracher (2015b, 2015c); Bracher et al. (2015b)
ANT25.1 (PS73)	Taylor et al. (2011a, 2011b)
ANT26.4 (PS75)	Bracher (2015c, 2015d); Bracher et al. (2015b)
ANT27.2 (PS77)	Bracher (2015d, 2015e); Trimborn et al. (2015)
ANT28.3 (PS79)	Bracher (2014a); Soppa et al. (2014)
MSM18	Bracher (2015a); Bracher et al. (2015b)
MSM09	Bracher and Taylor (2017)
SO202	Taylor and Bracher (2017); Zindler et al. (2013)
SO218	Bracher (2014b); Soppa et al. (2014)
SO234/235	Bracher et al. (2019); Booge et al. (2018)
SO243 (ASTRA)	Bracher (2019a); Booge et al. (2018)
PS93.2	Liu et al. (2018, 2019a)
PS99.2	Liu et al. (2018, 2019a)
PS107	Liu et al. (2019a, 2019b)
PS103	Bracher (2019b)
HE462	Bracher and Wiegmann (2019)
CLIVAR	*AEsOP*-CSIRO
BROKEWEST	*AEsOP*-CSIRO
Beagle (6 legs)	*AEsOP*-CSIRO
SOOP	*AEsOP*-CSIRO
SS (x6)	*AEsOP*-CSIRO
FR200001	*AEsOP*-CSIRO
TIP2000	*AEsOP*-CSIRO
NWS-jun03	*AEsOP*-CSIRO
Sniper (x4)	*AEsOP*-CSIRO
GBR (x5)	*AEsOP*-CSIRO

Model output provided physical variables, T and E, and biological variables by phytoplankton group, *Nlimit*, Chla, C, α_{NP} and α. The group-specific values were averaged considering the relative contribution of each group to total biomass to obtain the values for the whole phytoplankton community that we indicated with an overbar (see the supporting information for details on how we estimated community values for $\bar{\alpha}$ and $\bar{\alpha}_{NP}$ from several group-specific α's; Violle et al., 2007). Each output variable, including biological and physical, was averaged to a global 2° × 2° grid, within the 33 depth layers (0 to 5,750 m) used in Peloquin et al. (2013) and over 12 months. This resulted in a 4-D array per variable that had a common spatial and temporal resolution to be compared to observations (180 longitude × 90 latitude × 33 depth × 12 time).

3. Data

3.1. Satellite Observations

To test the consistency between the modeled and observed phytoplankton biomass, we considered climatologies of Chla and Chla:C from satellite observations between 2006 and 2010. Monthly means of surface Chla were obtained from the Ocean Colour Climate Change Initiative data set v3.0 by the European Space Agency (http://www.esa-oceancolour-cci.org/). We considered Chla concentration generated by SeaDAS using a blended combination of OCI (OC4v6 + Hu's CI), OC3, and OC5 depending on water class memberships (4,320 by 8,640 pixels, monthly means). Monthly means of surface Chla:C data were obtained from the Ocean Productivity Dataset by Oregon State University (http://www.science.oregonstate.edu/ocean.productivity/index.php). We considered Chla:C from the carbon-based productivity model (updated CbPM; Westberry et al., 2008) from MODIS r2018 (GSM) data (1,080 by 2,160 pixels, monthly means).

3.2. Accessory Pigments

Pigment data were obtained from published high-performance liquid chromatography data sets (Booge et al., 2018; Bracher et al., 2015b; Liu et al., 2018, 2019b; Peloquin et al., 2013; Soppa et al., 2014; Taylor et al., 2011a; Trimborn et al., 2015; Zindler et al., 2013), from pigment data in the *AEsOP*-CSIRO database (http://aesop.csiro.au/) and from two not previously published HPLC data sets (Table 4). These new data sets (Bracher, 2019b; Bracher & Wiegmann, 2019) encompassed the following cruises: the R/V Heincke cruise HE462 in the North Sea from 30 April to 7 May 2016 and the R/V Polarstern cruise PS103 in the South Atlantic from 17 December 2016 to 28 January 2017. During the cruises, 0.25 to 2.5 L of seawater was filtered through Whatman GF/F filters. The sample filters were then shock-frozen in liquid N_2 and kept at −80 °C until analysis. HPLC pigment analysis was performed following the method of Barlow et al. (1997) that was adjusted to our temperature-controlled instruments (Liu et al., 2019a; Taylor et al., 2011a). We determined the concentrations of pigments listed in Table 2 of Taylor et al. (2011a).

In all cases, TChla (micrograms per liter) encompassed all the reported Chla derivatives, monovinyl Chla, divinyl Chla, and chlorophyllide a. Total accessory pigment concentration (AP; micrograms per liter) was calculated as the summed concentration of all carotenoids and chlorophyll b and c. Carotenoids were grouped into photosynthetic (PSC; micrograms per liter) and photoprotective (PPC; micrograms per liter) carotenoids according to Aiken et al. (2009). PSC consisted of fucoxanthin (Fuco), peridinin (Perid), prasinoxanthin (Pras), 19'-hexanoyloxyfucoxanthin (Hex), and 19'-butanoyloxyfucoxanthin (But). As we focused on the long-term photoprotective response, both epoxidated and de-epoxidated states of xanthophylls were considered to be photoprotective and hence PPC consisted of alloxanthin (Allo), lutein (Lut), violaxanthin (Viola), zeaxanthin (Zea), diadinoxanthin (DD), diatoxanthin (DT), and alpha/beta-carotenes (Caro).

Within the compilation of pigment observations, the MAREDAT data set (Peloquin et al., 2013) was the most extensive. It was quality controlled by flagging (i) samples in which TChla was zero or less; (ii) samples in which fewer than four nonzero accessory pigments were reported; (iii) samples that fell outside the range of two standard deviations of the regression line of the log linear relationship between TChla and AP; and (iv) the entire campaign's samples if more than 35 % of samples from a given field campaign was flagged during the third step. However, not all cruises in MAREDAT provided concentrations of the full set of PPC pigments. In this case, we limited the analysis to the samples that contained measurements for the seven PPC pigments. This reduced the MAREDAT data set to 8,574 samples, that is, 25% of the quality-controlled data.

All the other data sets formed the NEW database in which all cruises provided the seven PPC. This NEW database was quality controlled independently following Aiken et al. (2009) by flagging (i) samples in which TChla was zero or less; (ii) samples where the difference of TChla and AP was more than 30% of the total pigment concentration; and (iii) the entire campaign's samples if the regression between TChla and AP have a slope outside the range 0.7–1.4, explain less than 90% of total variance or less than 85% of the samples of that particular cruise passed the previous criteria. This reduced the data set to 5,831 samples, that is, 89% of the original merged data.

All field data were gridded to the same 4-D array as described for model output. We obtained 1,985 grid points (404 in surface) in MAREDAT, and we used this set to derive a purely empirical parameterization of the relative PPC content from the physical forcing, *T*, *E*, and *Nlimit*, in the three modeling experiments. With NEW we obtained 2,086 grid points (789 in surface) that we used to validate the empirical predictions, as they were independent from MAREDAT. The combination of the two data sets (ALL) that encompassed 3,982 grid points (1,122 in surface) was used to test the mechanistic predictions in the experiment EXP-C.

To estimate the contribution of diatoms to TChla, we calculated the fraction of diatoms in Chla (fdChla) as 1.41xFuco/diagnostic pigment (DP) with D1.41Fuco + 1.41Perid + 1.27Hex + 0.6Allo + 0.35But + 1.01Chlb + 0.86Zea (Uitz et al., 2006). As an estimate of the contribution of the diatoms to the total pool of PPC, we considered the sum of DD and DT (micrograms per liter) as the photoprotective carotenoids in diatoms (Aiken et al., 2009; Strain et al., 1944). All other PPCs were considered to belong to nondiatoms.

4. Results

The analysis of results comprised three stages: (i) the prediction of PPC/TChla from model output, both empirically (from *E*, *T*, and *Nlimit*) and mechanistically (from $\bar{\alpha}$ and $\bar{\alpha}_{NP}$), (ii) the exploration of the spatial and temporal variability of PPC/TChla and the match between predictions and observations, and (iii) the analysis on the relative contribution of changes in community composition and physiological acclimation to the predicted PPC/TChla variability.

4.1. Prediction of PPC/TChla: Empirical and Mechanistic Approaches

We proposed a mechanistic approach of exploring photoprotection by comparing $\bar{\alpha}$ and $\bar{\alpha}_{NP}$. One can wonder if a simple empirical prediction of PPC/TChla from the model input variables was comparable to the mechanistic prediction. The empirical approach relied on the direct prediction of pigments from the input variables to the phytoplankton growth model, temperature, light, and nutrient availability, and hence, it can be fitted to all the three experiments. EXP-C was, however, the only experiment where the two types of predictions can be performed simultaneously. Hence, we used it to test the ability of the empirical and mechanistic approaches to match observations.

4.1.1. Empirical Prediction

The in situ pigment content in the MAREDAT data set was plotted against the physical input to the phytoplankton growth model (Figure 2). Individual pigment ratios relative to TChla were compared against a general rule of photoacclimation: Decreasing ratios with light are typical for light-harvesting pigments, and increasing ratios with light characterize photoprotective pigments (Henriksen et al., 2002; Schlüter et al., 2000). This was the case for all PSC (Fuco, But, Hex, Perid, and Pras) and for six of our PPC (Zea, Viola, DD, DT, Caro, and Lut). Allo, generally reported as photoprotective (Aiken et al., 2009; Henriksen et al., 2002; Schlüter et al., 2000), showed a decreasing ratio with increasing E. However, its contribution to the total pool of PPC was minimal. The ratios of the aggregated photosynthetic accessory pigments (PSPSC + Chlb + Chlc) and PPC, both relative to TChla, showed a comparable pattern as a function of *E*

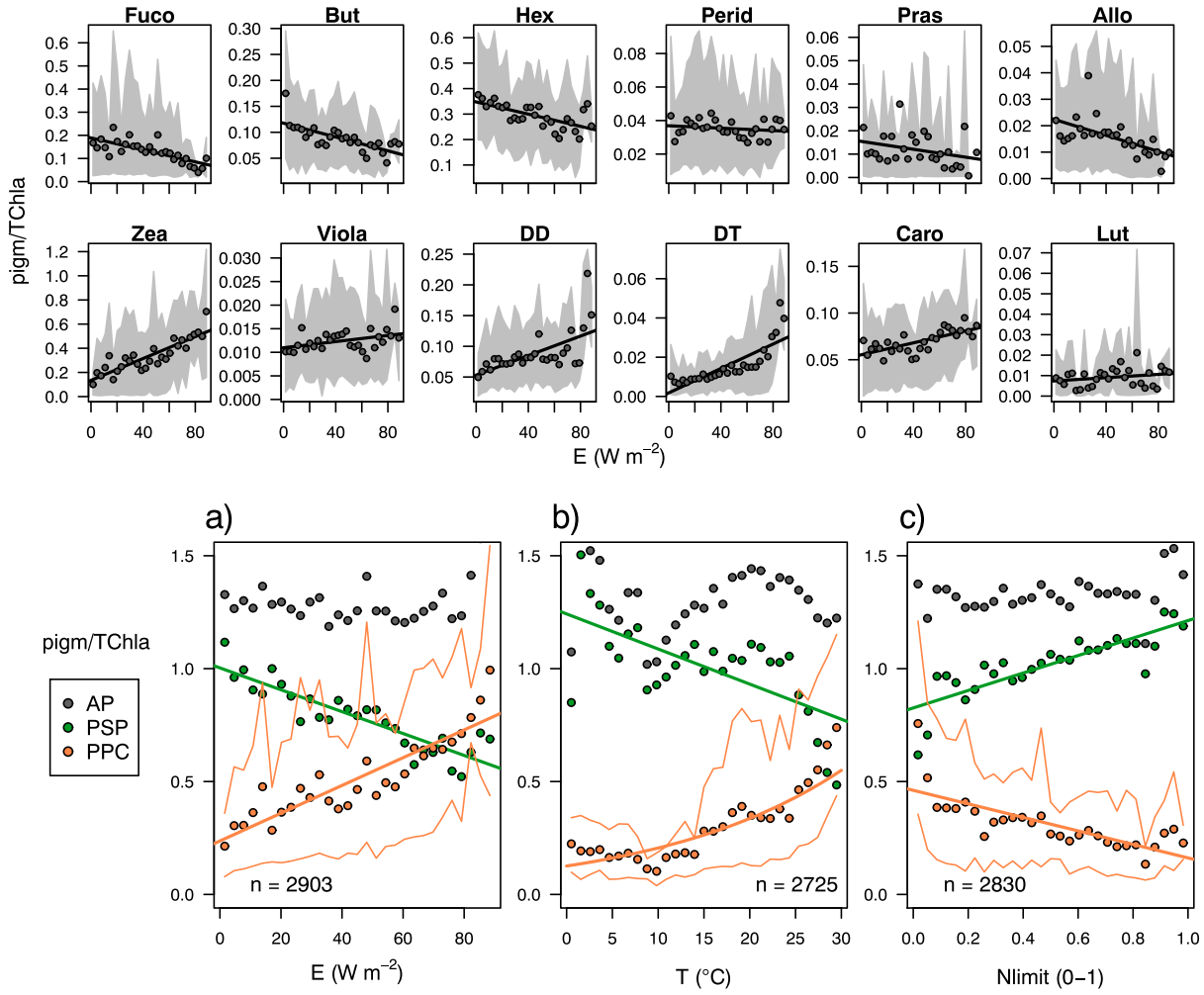

Figure 2. Variability of individual pigments to TChla ratios with light (small panels) and of total photoprotective (PPC), total photosynthetic accessory (PSP), and total accessory pigments (AP) with (a) light, (b) temperature, and (c) nutrient limitation in the EXP-C experiment. Dots indicate mean pigment ratios binned in *E*, *T*, and *Nlimit* classes, respectively. Solid lines show regression models fitted to binned data. Gray areas in the panels for individual pigments and narrow orange lines in the panels for aggregated pigments show percentiles 10 and 90 of the original range of pigment ratios.

(Figure 2a). This matched observed trends in the variation of PSP and xanthophyll's relative to Chla in numerous phytoplankton species (MacIntyre et al., 2002). PSP ad PPC ratios also followed inverse patterns with respect to *T* and *Nlimit* input variables. PSP content decreased with increasing *T* and nutrient limitation (limitation increases as Nlimit approaches 0) whereas PPC content responded opposed to that (Figures 2b and 2c).

The three input variables, *E*, *T*, *Nlimit*, and the interactions *E*:*T* and *E*:*Nlimit* had a significant effect on PPC/TChla (three-factor ANOVA, p value < 0.0001, $n = 2{,}830$), whereas the interactions *T*:*Nlimit* (p value $= 0.242$) and *E*:*T*:*Nlimit* (p value $= 0.447$) did not. Hence, we examined the ability to predict PPC/TChla through a simple empirical relationship that included all the three input variables as independent variables. To select the type of fit for each input variable, we binned pigments data in 30 *E*, *T*, and *Nlimit* classes, respectively. The best fit to the binned PPC/TChla data was linear for *E* (Figure 2a) but exponential for *T* (Figure 2b). Despite some deviation of the binned data at the extremes of *Nlimit*, PPC/TChla seemed to be reasonably well represented by a linear fit (Figure 2c). We fitted a multiple nonlinear model with nonlinear least squares method, function *nls* (Bates & Watts, 1988) in R (R Core Team, 2018). The resultant empirical model of PPC/TChla as a function of *E*, *T*, and *Nlimit* was PPC/TChla ~ 0.195 + 0.003 * *E* + (0.045 * exp(0.070 * *T*)) − 0.193 * *Nlimit*. We also fitted PPC/TChla to the input variables in the two other experiments, EXP-R and EXP-M. There were slight differences in the values of input variables among experiments, differences

Table 5
Skill Metrics per Experiment

Data set	Metric	EXP-R	EXP-M	EXP-C
log_{10}(Chla) (μg L^{-1})	R	0.648	0.649	0.644
(n=9491)	Bias	0.117	0.219	0.158
Chl:C (g:g)	R	0.514	0.520	0.517
(n=9401)	Bias	0.000	0.002	0.001
PPC:TChla NEW (g:g)	R	0.649	0.651	0.649
(n=747)	Bias	-0.015	-0.014	-0.014
PPC:TChla ALL (g:g)	R	-	-	0.663
(n=1082)	Bias	-	-	-0.020
NPP	PgC $year^{-1}$	35.59	33.84	36.21
ExportP	PgC $year^{-1}$	6.82	6.71	6.87

Note. Annual average correlations for log_{10}(Chla), Chla:C, and PPC/TChla at surface waters as compared to satellite OC-CCI Chla, satellite CbPM, and NEW (for empirical approach) or ALL (for mechanistic approach) HPLC data set, respectively. Also, total annual net primary production (NPP) and exported production (ExportP) integrated in the euphotic layer from the respective experiment are provided.

that were given by the effect of Chla on the attenuation of *E* and the effect of cellular quotas on *Nlimit*. Nevertheless, the differences in fitted coefficients and predictions were small, as shown by the similar metrics of the three empirical fits to observations of PPC/TChla (Table 5).

4.1.2. Mechanistic Prediction

Our approximation combining the models of Geider et al. (1998) and Marshall et al. (2000) provided both a maximum alpha ($\bar{\alpha}$) and the alpha that would appear under the effects of photodamage keeping the xanthophyll pigments pool constant ($\bar{\alpha}_{NP}$). $\bar{\alpha}$ was variable over the global oceans due to variable pigment composition in local phytoplankton communities adapted to varying nutrient and light limitation regimes. REcoM2 generated diversity in $\bar{\alpha}$ using constant group-specific α's and through changes in community composition (Figure 3a). This was a simplification but similar simple approximations have given good results when representing the variability of α in the global ocean (Arteaga et al., 2016). $\bar{\alpha}_{NP}$ was also variable over the global ocean and, overall, highlighted the areas where the risk of photoinhibition was higher (Figure 3b).

To further investigate how $\bar{\alpha}$ compared to $\bar{\alpha}_{NP}$ under the same conditions, we explored how $\bar{\alpha}$ and $\bar{\alpha}_{NP}$ varied as a function of light and nutrient limitation. With an increase in light and nutrient limitation, the community value of $\bar{\alpha}$ changed from a diatom-similar community to a small-phytoplankton-similar community, given a smaller prevalence of diatoms under such conditions (solid black line in Figure 4). $\bar{\alpha}_{NP}$ was close to $\bar{\alpha}$ under nutrient-replete and subsaturated light conditions, as represented in the central section of Figure 4, which indicates favorable conditions to keep a healthy light harvesting apparatus. When deviating from such favorable conditions, $\bar{\alpha}_{NP}$ decreased both with increasing light but also with increasing nutrient stress since repair mechanisms were nutrient limited (dotted lines in Figure 4).

The difference between $\bar{\alpha}$ and $\bar{\alpha}_{NP}$ under a particular set of environmental conditions reflected the degree of photoprotection necessary to keep $\bar{\alpha}_{NP}$ at the maximum value $\bar{\alpha}$. We expected that the difference between $\bar{\alpha}$ and $\bar{\alpha}_{NP}$ was somehow related to the amount of xanthophyll pigments in the case when photoprotection relied predominantly on photoprotective xanthophylls. The ratio between phytoplankton absorption computed without considering PPC and absorption computed considering all pigments has been used as a relative measure of the degree of photoprotection in phytoplankton (Lindley et al., 1995) and hence the amount of photoprotective pigments. We therefore proposed the ratio $\bar{\alpha}_{NP}/\bar{\alpha}$ as a proxy for the photoprotective gap in our model. When $\bar{\alpha}_{NP}/\bar{\alpha}$ was similar to one photodamage had a small impact on the light harvesting apparatus and hence the need for accumulating photoprotective pigments was small. Alternatively, an $\bar{\alpha}_{NP}/\bar{\alpha}$

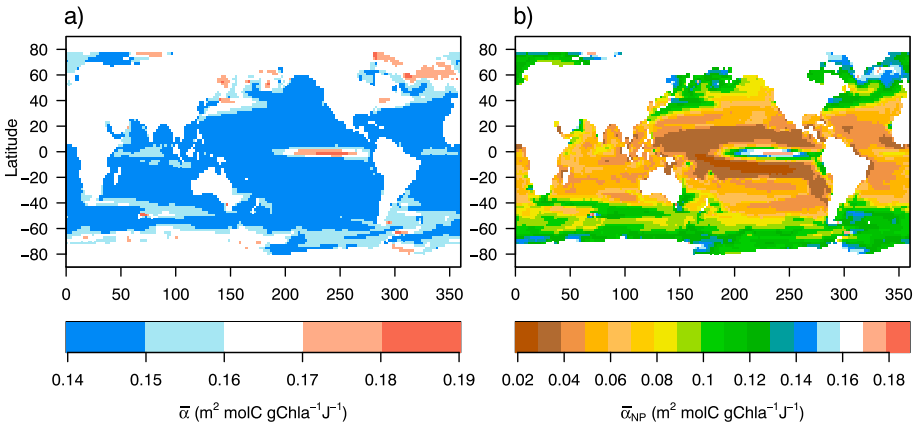

Figure 3. Variability of $\bar{\alpha}$ and $\bar{\alpha}_{NP}$ in the upper 15 m of the water column in the EXP-C experiment: (a) community $\bar{\alpha}$ as derived from standard REcoM2 based on Geider model and (b) $\bar{\alpha}_{NP}$ as derived from the Marshall model with constant xanthophyll pool.

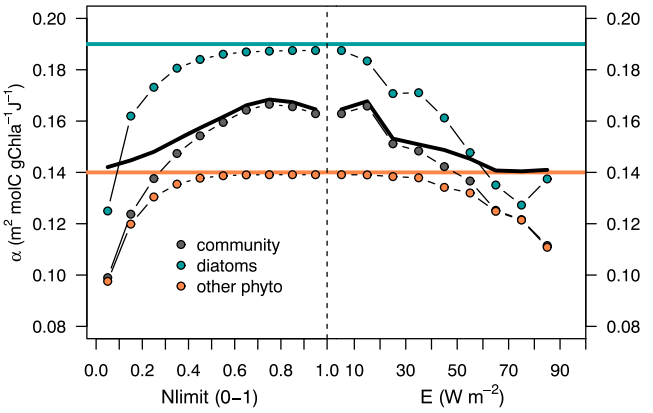

Figure 4. Variability of $\bar{\alpha}$ (lines) and $\bar{\alpha}_{NP}$ (dots) as a function of light (*E*) and nutrient limitation (*Nlimit*) in the EXP-C experiment. The orange and blue solid lines indicate α of undamaged PSII of diatoms and nondiatoms, respectively, and the black line indicates the community-aggregated value ($\bar{\alpha}$) that changes due to the relative contribution of diatoms and nondiatoms under different environmental conditions. Dotted lines indicate α_{NP} and $\bar{\alpha}_{NP}$ for the same groups.

smaller than one indicated that cells, without accumulating PPC or relying on other heat dissipating mechanisms, would be exposed to photodamage. We then used $1 - \bar{\alpha}_{NP}/\bar{\alpha}$ to predict the amount of accumulated xanthophylls that would avoid such photodamage and compared those predictions to observations of PPC/TChla.

4.1.3. Skill Metrics

To assess the predictions of the models against observations, we compared surface model results against log transformed Chla (micrograms per liter) from OC-CCI, Chl:C (in weight) from CbPM, and PPC/TChla (in weight) from the HPLC data sets, the latter sampled within 0- to 15-m depth. Correlation coefficients and average errors or bias (Stow et al., 2009) were computed for the three experiments EXP-R, EXP-M, and EXP-C, against the observational data sets. For each experiment, the empirical predictions of PPC/TChla were tested against the NEW data set, as this was independent from the MAREDAT data set used to fit the models. The mechanistic approach was only available for the experiment EXP-C, whose predictions were tested against the ALL data set. Results of these comparisons are presented in Table 5.

EXP-R predicted phytoplankton dynamics following Geider et al. (1998) with a photodamage-dependent loss term for Chla and provided Chla fields and Chl:C ratios well correlated to satellite derived observations (Álvarez et al., 2018). The inclusion of the original Marshall et al. (2000) model within REcoM2 (EXP-M), substituting $\bar{\alpha}$ with $\bar{\alpha}_{NP}$ in the P^{C}_{phot}-E curve, did not modify the correlation with surface log-transformed Chla or Chla:C significantly. Instead, it increased the bias of both estimates and decreased the total net primary production on an annual basis from 35.6 to 33.8 PgC/year. This showed that including details on the reversible regulation of PSII seems not to be relevant to predict Chla at global scale and may not be a high priority given the associated increase in computational costs.

The combined approach (EXP-C) provided comparable correlations and bias for Chla and Chl:C as EXP-R but allowed to predict PPC/TChla both empirically and mechanistically. The empirical predictions provided surface values of PPC/TChla highly correlated to observations, with a correlation coefficient of 0.649 and bias of −0.014. The mechanistic predictions that used $\bar{\alpha}$ for production and $\bar{\alpha}_{NP}/\bar{\alpha}$ as a proxy for photoprotection provided a correlation coefficient of 0.663 but a slightly larger bias of −0.020. Note, however, that the ALL data set against which we tested mechanistic predictions was larger than NEW.

4.2. Spatial and Temporal Variability of PPC/TChla

In this section, the empirical and mechanistic predictions of PPC/TChla for EXP-C were compared with HPLC field data. In surface waters (<15-m depth), field data (Figure 5a) showed high concentrations of PPC in tropical and subtropical areas with a decrease around the equator, which was very pronounced in the Pacific but also visible in the Atlantic (Lindley et al., 1995). Smaller values of PPC/TChla were obtained in temperate and polar waters. A comparable latitudinal pattern in PPC content has been reported by Bricaud et al. (2004). The empirical prediction of PPC/TChla showed the same latitudinal pattern with rather horizontal isolines (Figure 5b). The mechanistic prediction (Figure 5c) showed the latitudinal pattern, but with more longitudinal variability. The correlations in surface waters were almost identical for the two models when both were correlated to the NEW in situ data set, 0.649 for the empirical and 0.654 for the mechanistic. Mechanistic predictions showed a slightly larger bias (Table 5). Regardless of the latitudinal pattern, it was remarkable that in areas where the latitudinal pattern was not followed strictly, such as the upwellings of Morocco, Benguela, Peru, and Arabian sea, the mechanistic model matched the observations better than the empirical model, which suggested not-linear effects of nutrients, *T* and *E* on PPC/TChla ratios.

Observed and predicted PPC/TChla were compared for surface waters along a latitudinal gradient for the three major ocean basins (Figure 6). The reduced longitudinal variability of the empirical model was observed in the range of PPC/TChla values (orange areas in Figure 6) that did not cover the variability of field data at a given latitude. On the other hand, mechanistic predictions (blue areas in Figure 6) showed

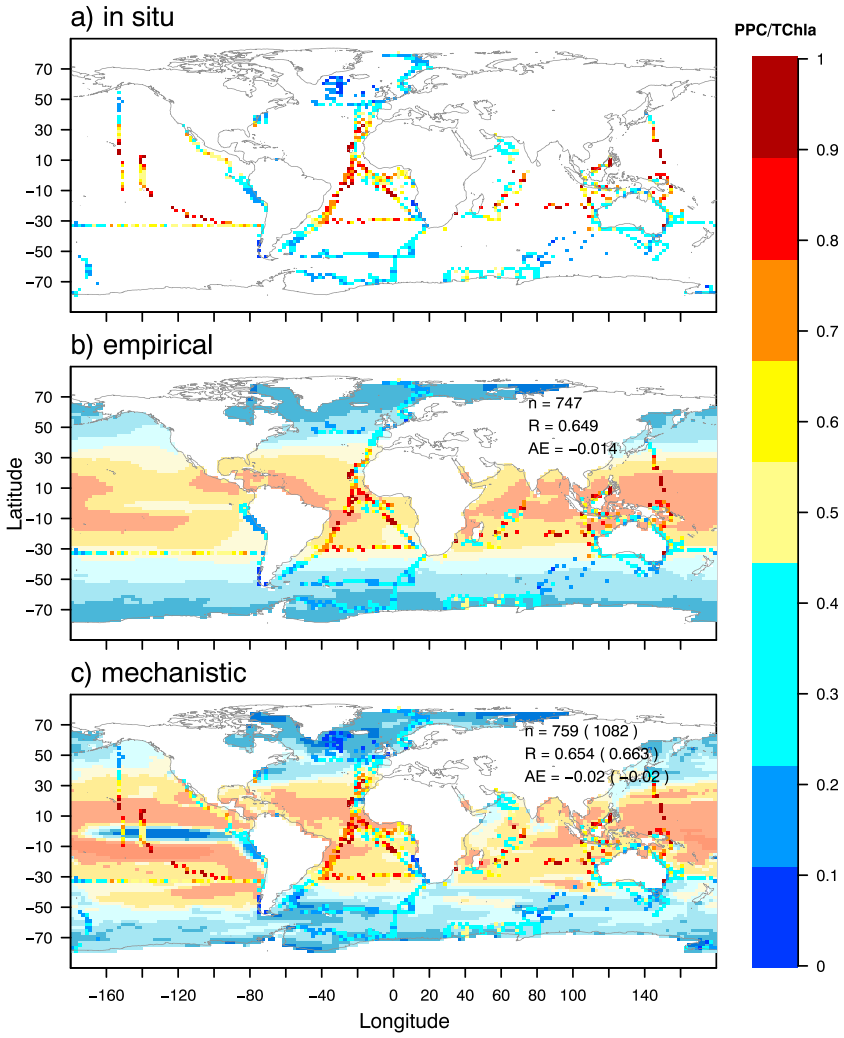

Figure 5. Photoprotective pigments in surface waters (averaged over the upper 15 m and scaled to 2° resolution): (a) PPC/TChla from HPLC data set ALL (also in c) and predicted (b) empirically and (c) mechanistically in the EXP-C experiment. Number of collocated observations (*n*), Person's correlation factor (*R*), and bias (*AE*) are shown for modeling predictions compared against NEW data set and against ALL data set within parenthesis in (c).

more variability and, hence, were able to predict PPC/TChla that did not simply follow a clear latitudinal gradient, as shown in the previous surface plots (Figure 5).

Zonal annual mean depth profiles of observed and predicted PPC/TChla showed that both types of predictions reproduced the in situ depth profiles (Figure 7). The field data showed a decrease of photoprotective pigments with depth in the entire tropical and subtropical ocean. In these areas, significant amounts of photoprotective pigments were observed close to the surface, but even at depths greater than 100 m, we found PPC/TChla ratios larger than 0.4. As expected due to the ambient light north and south of 40°, PPC presence was scarce, below 20% of TChla, but the gradient of decrease with depth was still visible (Figure 7a). The empirical model predicted this gradient quite precisely, although the values in surface tended to be smaller than the observations (Figure 7b). The gradient predicted by the mechanistic model was more abrupt, and values were much lower than observations at depths greater than 75 m. The values at the surface, as shown by previous figures, matched the observations well (Figure 7c). The occasional very high values at depths greater than 100 m in field samples at latitudes <40° were not reflected well in the predictions. While the empirical model predicted a low presence of pigments below 100 m (0.3 > PPC/TChla > 0.1), the mechanistic approach predicted a near absence down to this depth (PPC/TChla < 0.1). By observing

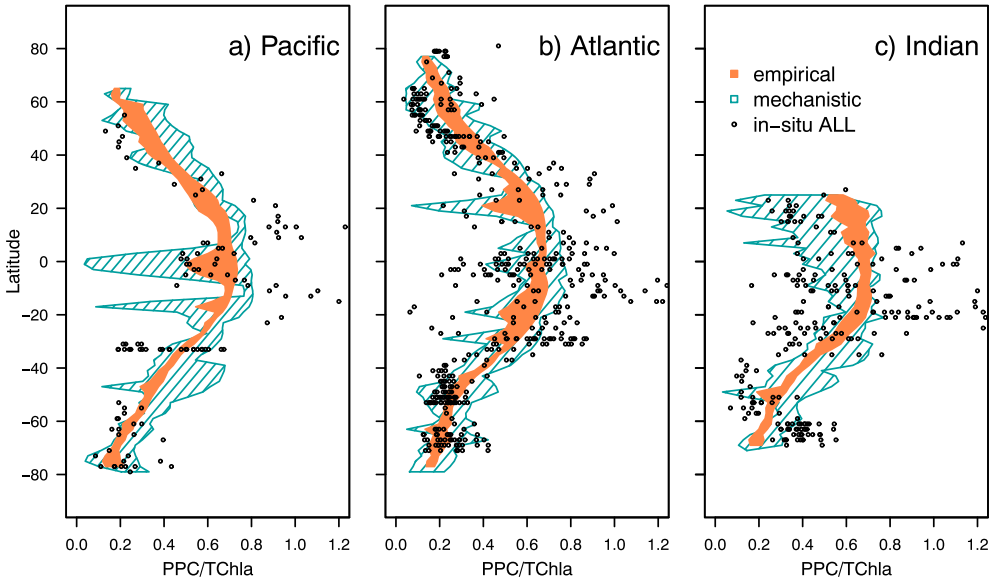

Figure 6. Latitudinal gradients of *in situ* (black dots) and predicted PPC/TChla values from the empirical and mechanistic approaches in the EXP-C experiment across surface waters of the (a) Pacific, (b) Atlantic, and (c) Indian Ocean.

the distribution of predicted TChla (white lines in Figure 7c), it was noticeable that high PPC/TChla values were predicted mainly for the phytoplankton living above the subsurface Chla maximum.

Averaged annual cycles of PPC/TChla predictions using the mechanistic approach (gray areas in Figure 8) showed a clear seasonality in temperate and high latitudes of both hemispheres (Figures 8a and 8c). In both cases, maximum values for the whole range of PPC/TChla occurred during summer and minimum values in

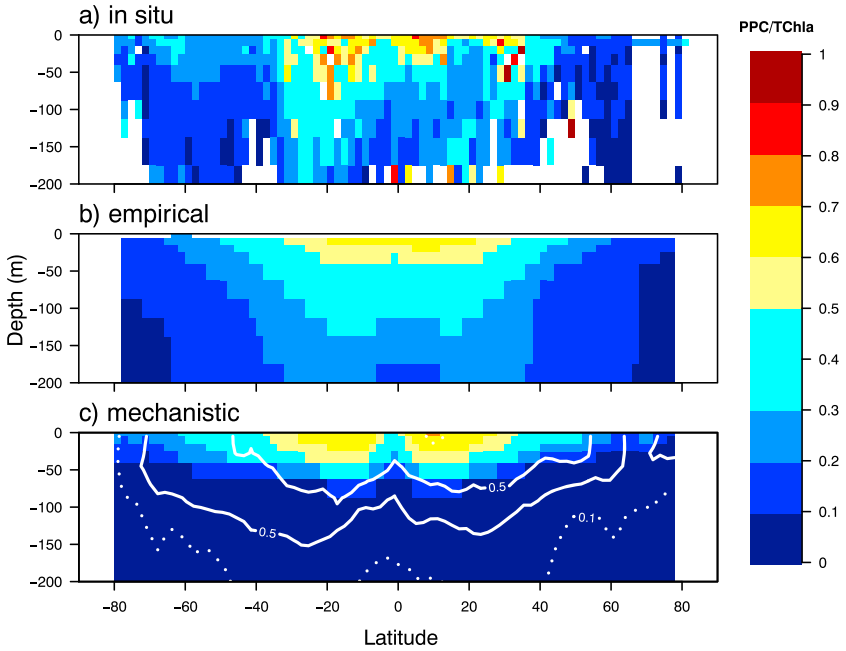

Figure 7. Zonal annual mean depth profiles of PPC/TChla as a function of latitude from (a) in situ HPLC ALL data set and predictions from (b) empirical and (c) mechanistic approaches in the EXP-C experiment. In panel (c) solid isolines show the predicted level of 0.5 μg Chla L^{-1} that enclose the subsurface Chla maximum and the dotted line shows the level of 0.1 μg Chla L^{-1}.

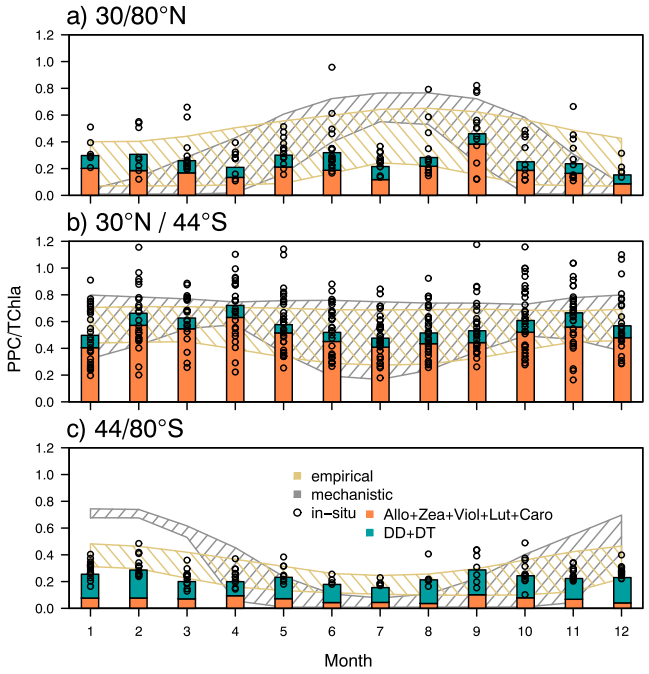

Figure 8. Averaged seasonal distribution of in situ (colored bars reflect the regional monthly average value of the specific PPC pigments and dots reflect the sum of all PPC pigments for each single data point in the respective region) and predicted (the range of values is given) PPC/TChla values in the EXP-C experiment for latitudes (a) north of 30°N, (b) between 30°N and 44°S, and (c) south of 44°S.

winter. In tropical and subtropical areas, the seasonality was only reflected in the range of the lowest values but constant for the maximum ones (Figure 8b). The empirical model predictions showed less seasonality in all regions, as they followed the observations where no seasonality for PPC/TChla was seen. The empirical predictions showed less variability than observations, which were better matched by the range of the mechanistic model predictions. Monthly mean values of in situ PPC/TChla (bars in Figure 8) were divided into the contribution of Allo, Viola, Lut, Zea, and Caro and the contribution of DD and DT. In high latitudes, where the contribution of diatoms was larger, the sum of DD+DT comprised an important proportion of PPC (Figure 8c).

4.3. Change in PPC/TChla: Effect of Community Composition and Physiological Acclimation

On an annual perspective, predicted PPC/TChla matched observations (Figures 5 and 6) or were lower (Figure 7), which indicated that the observed pool of PPC would be enough to cover the needs for photoprotection. Variations in community PPC content, however, can be driven by physiological acclimation as well as shifts in community composition. To explore which mechanism contributed more to the change in community PPC/TChla, both group-specific pigment content and a description of community composition were needed. This was challenging for observations because we did not have an independent estimate of community composition but the pigments themselves. The estimate of the contribution of diatoms to total chlorophyll relied on the use of DPs (Uitz et al., 2006; Figure 9a). Although the contribution of diatoms to total PPC pool can be illustrated with the sum DD+DT (Strain et al., 1944; Figure 9b), other groups can share the same pigments. This uncertainty could translate to the empirical model since it required a group-specific fit to observations to provide predictions for each individual group.

The advantage of the mechanistic approach in this context was that, in addition to predicting group specific pigment content, it provided a full description of community composition. Phytoplankton diversity represented by just two groups allowed us to build a description of the entire community composition by a single index of dominance that reflected the contribution of one of the groups to the total biomass. On an annual basis, the contribution of diatoms Chla to TChla (Figure 9c) and the contribution of diatom PPC to the total pool of PPC (Figure 9d) showed dominance of diatoms at the equator, high latitudes and near the eastern coasts of continents at midlatitudes.

In the absence of physiological acclimation that changes group-specific PPC/TChla ratios, dominance indexes (% of diatoms) in terms of TChla and in terms of PPC would vary in parallel. The variation over the year of the % of diatoms in terms of Chla, PPC, and also C were explored for nine areas of the world ocean (Figure 9). A noticeable difference between the time derivatives of the PPC- and Chla-based dominances (gray bars in Figure 9) indicated that the ratio PPC/TChla was variable within one or both phytoplankton groups. In the central areas of the Pacific, Atlantic, and Indian Oceans, dominance indexes varied in parallel, which indicated that changes in community PPC content were driven by changes in community composition. At higher latitudes, prior to the polar winter, PPC-based dominance changed faster than Chla-based dominance while prior to polar summer, PPC dominance changed slower than Chla-based dominance. Both phenomena implied intragroup acclimative changes in the PPC/TChla ratios.

5. Discussion

As in higher plants, most phytoplankton cells possess specialized carotenoid pigments that contribute to the rapid and harmless thermal dissipation of excess absorbed light energy in response to a sudden increase in irradiance (Demmig-Adams & Adams, 1992). This function reduces the excitation pressure on the reaction center of PSII and limit photoinhibition. Marshall et al. (2000) proposed a mechanistic model to describe

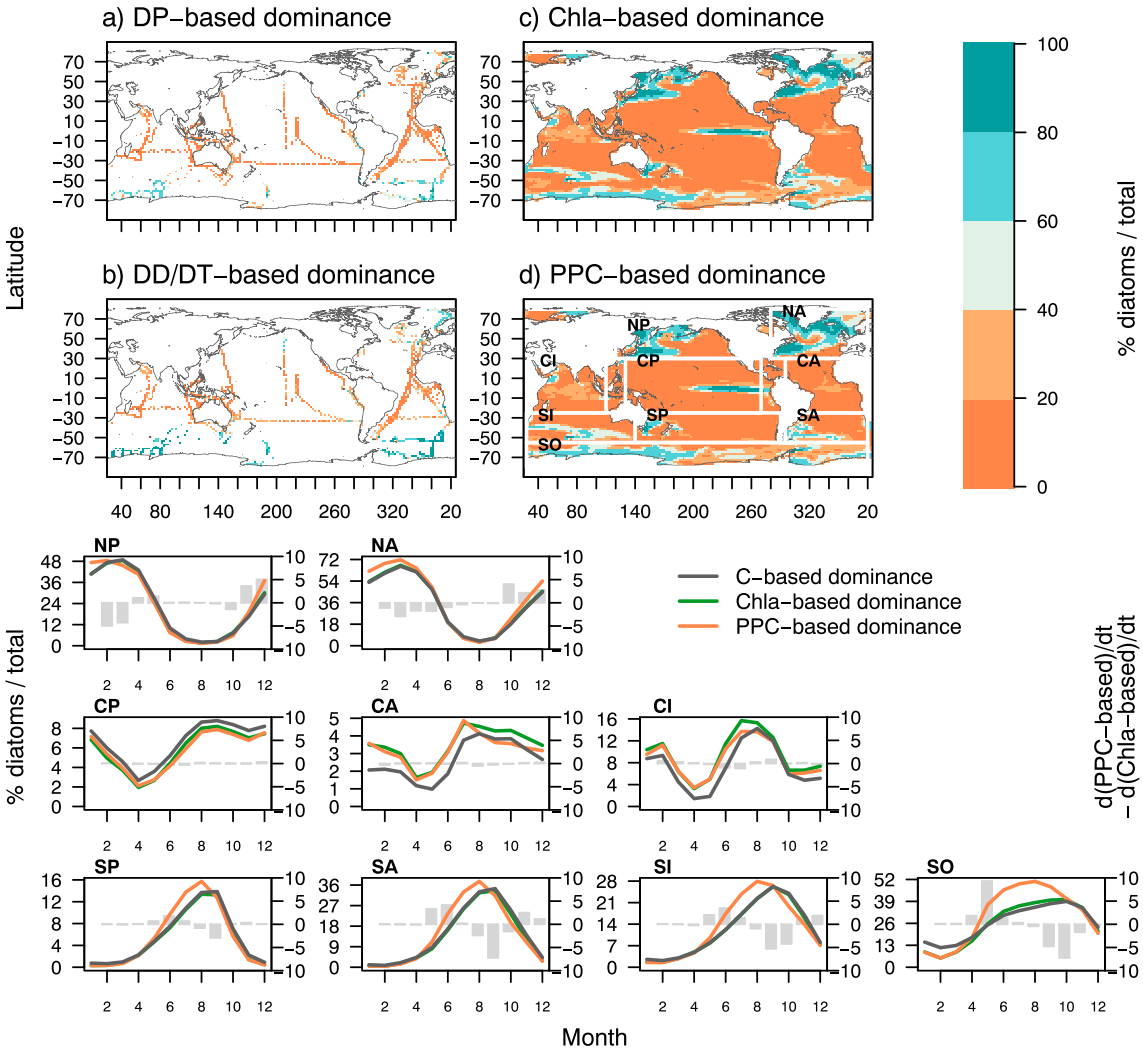

Figure 9. Observed contribution of diatoms (%) to total community in terms of (a) Chla derived from diagnostic pigments (from fd_{Chla}; Uitz et al., 2006) and (b) sum DD+DT to total PPC. Predicted contribution of diatoms (%) to total community in terms of (c) Chla and (d) PPC. Small panels show the variation along the year of C-, Chla-, and PPC-based dominance (% diatoms) in the nine ocean regions indicated in (d) left axis (note that the scale range is different for each panel). Gray bars show the difference between the time derivatives of the PPC-based and the Chla-based dominance (right axis, all using the same scale).

photoinhibition as a consequence of the decrease in the proportion of active PSII and the effect on the initial slope of the PE curve (α). Photoinhibition is expected to be small for natural phytoplankton communities acclimated to ambient light (Cullen et al., 1992), so we can assume that phytoplankton cells possess the mechanisms to keep α at a maximum value. Among these mechanisms, the presence of xanthophyll pigments is certainly expected to play a role since the thermal dissipation process is assisted by the nearly universal function of xanthophylls (Demmig-Adams & Adams, 1996). We therefore used the Marshall et al. (2000) model to estimate the extent of photoinhibition that phytoplankton communities would have to deal with. We explored whether the photoprotective role was performed by a variable pool of xanthophylls and whether the variability in the community xanthophyll pool was driven by shifts in community composition or implied intraspecific adjustments of pigment content.

5.1. Relevance of Photoprotective Pigments

Both this mechanistic and an empirical approach based on parallel in situ observations of PPC/TChla were able to predict the long-term photoprotective response and simulate the cellular accumulation of xanthophylls. The mechanistically determined need for photoprotection was in agreement with field observations of PPC/TChla in most of the surface ocean, at depth and even across seasons. This suggested a predominant

role of PPC in photoprotective activities in the global ocean with implications for the fast regulation of photosynthetic productivity and carbon fluxes in the ocean.

The approach presented allowed us to predict PPC content via modeling and hence provided a comprehensive description of pigment content of the phytoplankton community at the global scale provided by models. The content in photosynthetic pigments (Chla) and nonphotosynthetic pigments (PPC) relative to biomass (C) relates to the contribution of photochemical and nonphotochemical pathways, respectively, to the fate of absorbed light (Lin et al., 2016). Knowledge of full pigment signatures is crucial for understanding the coupling of light absorption to carbon fixation in the ocean.

5.2. Relevance of Other Physiological Mechanisms

Discrepancies between the mechanistically determined need for photoprotection and observations of PPC/TChla highlighted scenarios where PPC content was apparently insufficient to protect the community and thus other mechanisms of NPQ became relevant for heat dissipation. Particularly during summer season at high latitudes (Figure 8), the amount of PPC fell below the needs for photoprotection, suggesting that in these areas alternative mechanisms may be relevant for photoprotection.

The difference between predictions and observations can be explained by simplifications of the model framework. A functional classification of carotenoids into two groups of pigments, photosynthetic and photoprotective, is commonly used in the literature (e.g., Bidigare et al., 1990). However, in some groups, the photosynthetic pigment fucoxanthin may be converted to DD relatively quickly (Harris et al., 2009; Polimene et al., 2012), thus giving fucoxanthin a role in long-term photoprotection. Also, the effectiveness of the XC varies across taxa (Goss & Jakob, 2010; Lavaud, 2007; Six et al., 2009), which can lead to smaller PPC content in communities dominated by groups containing more efficient XC. In addition to pigments, energy dissipation can be covered by other protective mechanisms not explicitly considered here, such as fluorescence or constitutive heat dissipation (Porcar-Castell et al., 2006). Autotrophic cells also possess some plasticity to reorganize their photochemical pathways when the photochemical capacity is exceeded, performing cyclic electron flow around PSII (Goss & Lepetit, 2015) or alternative electron transport (Wagner et al., 2006).

5.3. Change in PPC Content: Intragroup Acclimation or Shifts in Community Composition

Given that results showed that variable PPC/TChla ratios covered most of phytoplankton photoprotective needs, the question that arose next was whether this variability in pigment content was driven by shifts in community composition or implied physiological acclimation within a given group. The mechanistic approach proposed provided the two elements, which are necessary to tackle this question: group-specific PPC predictions and a complete description of community composition.

Group-specific photoprotective needs were generated by assigning smaller damage coefficients to diatoms than to other phytoplankton, larger photochemical efficiency to diatoms, and equal absorption cross-sections and repair rates to both groups. Although the variability in the predictions was high for both groups, the predicted needs for photoprotection tended to be higher in other phytoplankton than in diatoms. This corresponds to the observation that smaller phytoplankton can grow in a high but relatively constant light environment where they do not need to invest as heavily in photosynthetic machinery but require mechanisms to reduce the harmful effect of extensive periods of excess irradiance (Kropuenske et al., 2009). Smaller phytoplankton like prasinophytes cope with prolonged stress and subsequent recovery through a large induction and relaxation of XC-induced NPQ (Liefer et al., 2018). Diatoms on the other hand show lower susceptibility to photoinactivation of PSII (Key et al., 2010) and rely on constitutive dissipation of excitation energy more than on XC NPQ (Liefer et al., 2018).

Identification of microalgae species through diagnostic pigments implies the assumption that changes in community accessory pigments are solely driven by changes in community composition. This is reasonable when the pigment ratios are constant in time for a particular species. However, variations in diagnostic pigments to Chla ratios also arise due to factors such as nutrient status and light (Mackey et al., 1996). Our results showed that, for most of the tropical and subtropical ocean, photoprotective pigments dominated photoprotection and changes in total photoprotective pigments were caused mainly by taxonomic changes within the phytoplankton community. Our results also highlighted scenarios at high latitudes where changes in PPC content can also result both from shifts in community composition and from

photoacclimation within the same community. During polar winter, in absence of nutrient limitation, physiological acclimation took place and contributed to changes in PPC/TChla ratios (Figure 9) that met photoprotective needs (Figures 8a and 8c).

5.4. The Role of Nutrients and Temperature on High-Latitude Photoprotection

During polar summer, the high requirement of photoprotection predicted by our mechanistic approach was not observed in field measured PPC/TChla (Figures 8a and 8c). At the same time, there was no sign of physiological acclimation (Figure 9). This suggested not only that other mechanisms of photoprotection may be more relevant than PPC-mediated mechanisms in these areas but also that PPC synthesis itself was limited. The observed physiological acclimation during winter when nutrients were replenished and temperatures were low suggested that nutrients and not temperature limited the use of PPC-based NPQ in those polar areas during the summer season. Under incomplete photoprotection provided by other mechanisms, net photodamage could eventually occur since the repair of damaged photosystems was both nutrient and temperature limited. In a previous application of the REcoM2 model, we showed that given the nutrient requirements of repair mechanisms, severe nutrient stress translates into photoinhibition of the light harvesting apparatus in the absence of complete photoprotection (Álvarez et al., 2018). Since it has been observed that photodamage can shape the phytoplankton community in the Southern Ocean (Alderkamp et al., 2010), our results show that nutrient limitation of PSII repair and/or PPC de novo synthesis may be the cause of these photoinhibitory responses at high latitudes.

6. Conclusions

This study suggests that a variable pool of xanthophyll pigments mediates the long-term photoprotective responses of phytoplankton throughout most of the ocean. Hence, the photoprotective pigments accumulated by phytoplankton can be accurately predictable by models. This potentially provides a comprehensive view of the phytoplankton community pigment signature in terms of photosynthetic and nonphotosynthetic pigments, which is crucial for modeling the coupling of light absorption to carbon fixation in the ocean. The variability in the pool of xanthophyll pigments seems to be driven mainly by changes in community composition in the tropical and subtropical ocean, and in these areas pigment composition may reflect taxonomic composition strongly. At higher latitudes, during the nutrient-limited summer season, photoprotection needs do not seem to be met by changes in xanthophyll pigments and must be met by other energy-dissipating mechanisms. When nutrients are resupplied and the nutrient limitation of pigment synthesis relaxes, both taxonomic shifts and intraspecific photoacclimation appear to shape community pigment signature. These insights about how much of the variability in community nonphotosynthetic pigments is attributable to changes in community composition or changes in physiological state may allow an improvement of the match between remotely sensed optical data and the underlying phytoplankton community.

Acknowledgments
This work is a contribution to the IPSO project "Improving the prediction of photophysiology in the Southern Ocean by accounting for iron limitation, optical properties and spectral satellite data information" funded by the Alfred Wegener Institute. A. B.'s contribution is partly supported by the Transregional Collaborative Research Center (TR 172) "ArctiC Amplification: Climate Relevant Atmospheric and SurfaCe Processes, and Feedback Mechanisms (AC)3" via the subproject C03. Y. L.'s contribution is supported with a PhD fellowship by the China Scholarship Council. For HPLC analysis of filters sampled at PS103 and HE462, we thank Sonja Wiegmann, and for supporting the water sampling and filtration at these cruises, we thank Rafael Goncalves Araujo and Julia Oelker (PS103), and Sebastian Hellman and Sonja Wiegmann (HE462). We also thank the captains and the crews, especially the chief scientists Olaf Boebel (PS103), Thomas Soltwedel (PS107), and Sören Kraegevsky (HE462), for their support. We thank two anonymous reviewers for their helpful and constructive comments that improved the manuscript. All field data used in this work and listed in Table 4 are publicly available in PANGAEA under the url's included in the references list and in the AEsOP database (under http://aesop.csiro.au/).

References

Aiken, J., Pradhan, Y., Barlow, R., Lavender, S., Poulton, A., Holligan, P., & Hardman-Mountford, N. (2009). Phytoplankton pigments and functional types in the Atlantic Ocean: A decadal assessment, 1995-2005. *Deep-Sea Research Part II: Topical Studies in Oceanography*, *56*(15), 899–917. https://doi.org/10.1016/j.dsr2.2008.09.017

Alderkamp, A.-C., de Baar, H. J. W., Visser, R. J. W., & Arrigo, K. R. (2010). Can photoinhibition control phytoplankton abundance in deeply mixed water columns of the Southern Ocean? *Limnology and Oceanography*, *55*(3), 1248–1264. https://doi.org/10.4319/lo.2010.55.3.1248

Álvarez, E., Thoms, S., & Völker, C. (2018). Chlorophyll to carbon ratio derived from a global ecosystem model with photodamage. *Global Biogeochemical Cycles*, *32*, 799–816. https://doi.org/10.1029/2017GB005850

Antonov, J. I., Seidov, D., Boyer, T. P., Locarnini, R. A., Mishonov, A. V., Garcia, H. E., et al. (2010). World Ocean Atlas 2009, volume 2: Salinity, 40 pp. In S. Levitus (Ed.), NOAA Atlas NESDIS 69 (pp. 184). Washington, DC: U.S. Gov. Printing Office.

Arteaga, L., Pahlow, M., & Oschlies, A. (2016). Modeled Chl:C ratio and derived estimates of phytoplankton carbon biomass and its contribution to total particulate organic carbon in the global surface ocean. *Global Biogeochemical Cycles*, *30*, 1791–1810. https://doi.org/10.1002/2016GB005458

Aumont, O., Maier-Reimer, E., Blain, S., & Monfray, P. (2003). An ecosystem model of the global ocean including Fe, Si, P colimitations. *Global Biogeochemical Cycles*, *17*(2), 1060. https://doi.org/10.1029/2001GB001745

Babin, M., Morel, A., Claustre, H., Bricaud, A., Kolber, Z., & Falkowski, P. G. (1996). Nitrogen- and irradiance-dependent variations of the maximum quantum yield of carbon fixation in eutrophic, mesotrophic and oligotrophic marine systems. *Deep-Sea Research Part I: Oceanographic Research Papers*, *43*(8), 1241–1272. https://doi.org/10.1016/0967-0637(96)00058-1

Baird, M., Mongin, M., Rizwi, F., Bay, L., Cantin, N., Skerratt, J., & Soja-Wozniak, M. (2018). A mechanistic model of coral bleaching due to temperature-mediated light-driven reactive oxygen build-up in zooxanthellae. *Ecological Modelling*, *386*, 20–37. https://doi.org/10.31230/osf.io/etjd6

Barlow, R. G., Cummings, D. G., & Gibb, S. W. (1997). Improved resolution of mono- and divinyl chlorophylls a and b and zeaxanthin and lutein in phytoplankton extracts using reverse phase C-8 HPLC. *Marine Ecology Progress Series*, *161*, 303–307. https://doi.org/10.3354/meps161303

Bates, D. M., & Watts, D. G. (1988). Nonlinear Regression: Iterative Estimation and Linear Approximations. In D. M. Bates & D. G. Watts (Eds.), *Nonlinear Regression Analysis and Its Applications*. https://doi.org/10.1002/9780470316757.ch2

Bidigare, R. R., Ondrusek, M. E., Morrow, J. H., & Kiefer, D. A. (1990). In-vivo absorption properties of algal pigments. In *Proc. SPIE 1302, Ocean Optics X*, (pp. 556–565). Orlando, FL: 1990 Technical Symposium on Optics, Electro-Optics, and Sensors. https://doi.org/10.1117/12.21451

Booge, D., Schlundt, C., Bracher, A., Endres, S., Zäncker, B., & Marandino, C. A. (2018). Marine isoprene production and consumption in the mixed layer of the surface ocean—A field study over two oceanic regions. *Biogeosciences*, *15*(2), 649–667. https://doi.org/10.5194/bg-15-649-2018

Bracher, A. (2014a). Phytoplankton pigment concentrations during POLARSTERN cruise ANT-XXVIII/3. *PANGAEA*. https://doi.org/10.1594/PANGAEA.848588

Bracher, A. (2014b). Phytoplankton pigments measured on water bottle samples during SONNE cruise SO218. *PANGAEA*. https://doi.org/10.1594/PANGAEA.848589

Bracher, A. (2015a). Phytoplankton pigment concentrations during Maria S. Merian cruise MSM18/3. *PANGAEA*. https://doi.org/10.1594/PANGAEA.848586

Bracher, A. (2015b). Phytoplankton pigment concentrations during POLARSTERN cruise ANT-XXIV/1. *PANGAEA*. https://doi.org/10.1594/PANGAEA.848583

Bracher, A. (2015c). Phytoplankton pigment concentrations during POLARSTERN cruise ANT-XXIV/4. *PANGAEA*. https://doi.org/10.1594/PANGAEA.848584

Bracher, A. (2015d). Phytoplankton pigment concentrations during POLARSTERN cruise ANT-XXVI/4. *PANGAEA*. https://doi.org/10.1594/PANGAEA.848585

Bracher, A. (2015e). Phytoplankton pigment concentrations during POLARSTERN cruise ANT-XXVII/2. *PANGAEA*. https://doi.org/10.1594/PANGAEA.848590

Bracher, A. (2019a). Phytoplankton pigment concentrations during RV Sonne cruise SO243. *PANGAEA*. https://doi.org/10.1594/PANGAEA.898920

Bracher, A. (2019b). Phytoplankton pigment concentrations in the Southern Ocean during RV Polarstern cruise PS103 in Dec 2016 to Jan 2017. *PANGAEA*. https://doi.org/10.1594/PANGAEA.898941

Bracher, A., Cheah, W., & Wiegmann, S. (2019). Phytoplankton pigment concentrations in the tropical Indian Ocean in July and August 2014 during RV Sonne cruises SO234 and SO235. *PANGAEA*. https://doi.org/10.1594/PANGAEA.898929

Bracher, A., & Taylor, B. B. (2017). Phytoplankton pigment concentrations measured by HPLC during Maria S. Merian cruise MSM9/1. *PANGAEA*. https://doi.org/10.1594/PANGAEA.873070

Bracher, A., Taylor, M. H., Taylor, B. B., Dinter, T., Röttgers, R., & Steinmetz, F. (2015a). Phytoplankton pigment concentrations during POLARSTERN cruise ANT-XXIII/1. *PANGAEA*. https://doi.org/10.1594/PANGAEA.871713

Bracher, A., Taylor, M. H., Taylor, B. B., Dinter, T., Röttgers, R., & Steinmetz, F. (2015b). Using empirical orthogonal functions derived from remote-sensing reflectance for the prediction of phytoplankton pigment concentrations. *Ocean Science*, *11*(1), 139–158. https://doi.org/10.5194/os-11-139-2015

Bracher, A., & Wiegmann, S. (2019). Heincke Cruise HE462 phytoplankton pigments determined by HPLC. *PANGAEA*. https://doi.org/10.1594/PANGAEA.899043

Bricaud, A., Claustre, H., Ras, J., & Oubelkheir, K. (2004). Natural variability of phytoplanktonic absorption in oceanic waters: Influence of the size structure of algal populations. *Journal of Geophysical Research*, *109*, C11010. https://doi.org/10.1029/2004JC002419

Brunet, C., Johnsen, G., Lavaud, J., & Roy, S. (2011). Pigments and photoacclimation processes. In S. Roy, C. Llewellyn, E. Skarstad Egeland, & G. Johnsen (Eds.), *Phytoplankton Pigments, Characterization, Chemotaxonomy and Application in Oceanography*, (pp. 445–454). Cambridge: Cambridge University Press. https://doi.org/10.1017/CBO9780511732263.017

Brunet, C., & Lavaud, J. (2010). Can the xanthophyll cycle help extract the essence of the microalgal functional response to a variable light environment? *Journal of Plankton Research*, *32*(12), 1609–1617. https://doi.org/10.1093/plankt/fbq104

Campbell, D. A., & Tyystjärvi, E. (2012). Parameterization of photosystem II photoinactivation and repair. *Biochimica et Biophysica Acta-Bioenergetics*, *1817*(1), 258–265. https://doi.org/10.1016/j.bbabio.2011.04.010

Cullen, J. J., Yang, X., & MacIntyre, H. L. (1992). Nutrient limitation of marine photosynthesis. In P. G. Falkowski, & A. D. Woodhead (Eds.), *Primary Productivity and Biogeochemical Cycles in the Sea*, (pp. 70–88). New York: Springer. https://doi.org/10.1007/978-1-4899-0762-2_5

Demers, S., Roy, S., Gagnon, R., & Vignault, C. (1991). Rapid light-induced changes in cell fluorescence and in xanthophyll-cycle pigments of Alexandrium excavatum (Dinophyceae) and Thalassiosira pseudonana (Bacillario-phyceae): A photo-protection mechanism. *Marine Ecology Progress Series*, *76*, 185–193. https://doi.org/10.3354/meps076185

Demmig-Adams, B., & Adams, W. W. (1992). Responses of plants to high light stress. *Annual Review of Plant Physiology and Plant Molecular Biology*, *43*(1), 599–626. https://doi.org/10.1146/annurev.pp.43.060192.003123

Demmig-Adams, B., & Adams, W. W. (1996). The role of xanthophyll cycle carotenoids in the protection of photosynthesis. *Trends in Plant Science*, *1*(1), 21–26. https://doi.org/10.1016/S1360-1385(96)80019-7

Du, N., Gholami, P., Kline, D. I., DuPont, C. L., Dickson, A. G., Mendola, D., et al. (2018). Simultaneous quantum yield measurements of carbon uptake and oxygen evolution in microalgal cultures. *PLoS ONE*, *13*(6), e0199125. https://doi.org/10.1371/journal.pone.0199125

Dubinsky, Z., & Schofield, O. (2010). From the light to the darkness: Thriving at the light extremes in the oceans. *Hydrobiologia*, *639*(1), 153–171. https://doi.org/10.1007/s10750-009-0026-0

Dubinsky, Z., & Stambler, N. (2009). Photoacclimation processes in phytoplankton: Mechanisms, consequences, and applications. *Aquatic Microbial Ecology*, *56*, 163–176. https://doi.org/10.3354/ame01345

Flynn, K. J., & Flynn, K. (1998). Release of nitrite by marine dinoagellates: Development of a mathematical simulation. *Marine Biology*, *130*(3), 455–470. https://doi.org/10.1007/s002270050266

Flynn, K. J., Page, S., Wood, G., & Hipkin, C. R. (1999). Variations in the maximum transport rates for ammonium and nitrate in the prymnesiophyte Emiliania huxleyi and the raphidophyte Heterosigma carterae. *Journal of Plankton Research*, *21*(2), 355–371. https://doi.org/10.1093/plankt/21.2.355

Fujiki, T., & Taguchi, S. (2001). Relationship between light absorption and the xanthophyll-cycle pigments in marine diatoms. *Plankton Biology and Ecology*, *48*(2), 96–103.

Garcia, H. E., Locarnini, R. A., Boyer, T. P., Antonov, J. I., Zweng, M. M., Baranova, O. K., & Johnson, D. R. (2010). World Ocean Atlas 2009, Volume 4: Nutrients (phosphate, nitrate, and silicate), 26 pp. In *NOAA Atlas NESDIS 71*. Washington, DC: U.S. Government Printing Office. 398 pp.

Geider, R. J., MacIntyre, H. L., & Kana, T. M. (1997). Dynamic model of phytoplankton growth and acclimation: Responses of the balanced growth rate and the chlorophyll a:carbon ratio to light, nutrient-limitation and temperature. *Marine Ecology Progress Series*, *148*(1–3), 187–200. https://doi.org/10.3354/meps148187

Geider, R. J., MacIntyre, H. L., & Kana, T. M. (1998). A dynamic regulatory model of phytoplanktonic acclimation to light, nutrients, and temperature. *Limnology and Oceanography*, *43*(4), 679–694. https://doi.org/10.4319/lo.1998.43.4.0679

Goss, R., & Jakob, T. (2010). Regulation and function of xanthophyll cycle-dependent photoprotection in algae. *Photosynthesis Research*, *106*(1-2), 103–122. https://doi.org/10.1007/s11120-010-9536-x

Goss, R., & Lepetit, B. (2015). Biodiversity of NPQ. *Journal of Plant Physiology*, *172*, 13–32. https://doi.org/10.1016/j.jplph.2014.03.004

Gustafsson, M. S. M., Baird, M. E., & Ralph, P. J. (2014). Modeling photoinhibition-driven bleaching in Scleractinian coral as a function of light, temperature, and heterotrophy. *Limnology and Oceanography*, *59*(2), 603–622. https://doi.org/10.4319/lo.2014.59.2.0603

Han, B.-P. (2002). A mechanistic model of algal photoinhibition induced by photodamage to photosystem-II. *Journal of Theoretical Biology*, *214*(4), 519–527. https://doi.org/10.1006/jtbi.2001.2468

Han, B.-P., Virtane, M., Koponen, J., & Straskraba, M. (2000). Effect of photoinhibition on algal photosynthesis: a dynamic model. *Journal of Plankton Research*, *22*(5), 865–885. https://doi.org/10.1093/plankt/22.5.865

Harris, G. N., Scanlan, D. J., & Geider, R. J. (2009). Responses of Emiliania huxleyi (Prymnesiophyceae) to step changes in photon flux density. *European Journal of Phycology*, *44*(1), 31–48. https://doi.org/10.1080/09670260802233460

Hauck, J., Völker, C., Wang, T., Hoppema, M., Losch, M., & Wolf-Gladrow, D. A. (2013). Seasonally different carbon flux changes in the Southern Ocean in response to the southern annular mode. *Global Biogeochem Cycles*, *27*, 1236–1245. https://doi.org/10.1002/2013GB004600

Henriksen, P., Riemann, B., Kaas, H., Sorensen, H. L. H. M., & Sørensen, H. M. H. L. (2002). Effects of nutrient-limitation and irradiance on marine phytoplankton pigments. *Journal of Plankton Research*, *24*(9), 835–858. https://doi.org/10.1093/plankt/24.9.835

Hohn, S. (2009). Coupling and decoupling of biogeochemical cycles in marine ecosystems (Ph.D Thesis). Universität Bremen.

Horton, P., Ruban, A. V., & Wentworth, M. (2000). Allosteric regulation of the light-harvesting system of photosystem II. *Philosophical Transactions of the Royal Society B: Biological Sciences*, *355*(1402), 1361–1370. https://doi.org/10.1098/rstb.2000.0698

Jahns, P., Latowski, D., & Strzalka, K. (2009). Mechanism and regulation of the violaxanthin cycle: The role of antenna proteins and membrane lipids. *Biochimica et Biophysica Acta-Bioenergetics*, *1787*(1), 3–14. https://doi.org/10.1016/j.bbabio.2008.09.013

Key, R. M., Kozyr, A., Sabine, C. L., Lee, K., Wanninkhof, R., Bullister, J. L., et al. (2004). A global ocean carbon climatology: Results from GLODAP. *Global Biogeochemical Cycles*, *18*, GB4031. https://doi.org/10.1029/2004GB002247

Key, T., McCarthy, A., Campbell, D. A., Six, C., Roy, S., & Finkel, Z. V. (2010). Cell size trade-offs govern light exploitation strategies in marine phytoplankton. *Environmental Microbiology*, *12*(1), 95–104. https://doi.org/10.1111/j.1462-2920.2009.02046.x

Kiefer, D. A., & Mitchell, B. G. (1983). A simple steady state description of phytoplankton growth based on absorption cross section and quantum efficiency. *Limnology and Oceanography*, *28*(4), 770–776. https://doi.org/10.4319/lo.1983.28.4.0770

Kolber, Z., Zehr, J., & Falkowski, P. (1988). Effects of growth irradiance and nitrogen limitation on photosynthetic energy conversion in photosystem II. *Plant Physiology*, *88*(3), 923–929. https://doi.org/10.1104/pp.88.3.923

Kromkamp, J. C., Domin, A., Dubinsky, Z., Lehmann, C., & Schanz, F. (2001). Changes in photosynthetic properties measured by oxygen evolution and variable chlorophyll fluorescence in a simulated entrainment experiment with the cyanobacterium Planktothrix rubescens. *Aquatic Sciences*, *63*(3), 363–382. https://doi.org/10.1007/PL00001360

Kropuenske, L. R., Mills, M. M., van Dijken, G. L., Bailey, S., Robinson, D. H., Welschmeyer, N. A., & Arrigoa, K. R. (2009). Photophysiology in two major Southern Ocean phytoplankton taxa: Photoprotection in *Phaeocystis antarctica* and *Fragilariopsis cylindrus*. *Limnology and Oceanography*, *54*(4), 1176–1196. https://doi.org/10.4319/lo.2009.54.4.1176

Lavaud, J. (2007). Fast regulation of photosynthesis in diatoms: Mechanisms, evolution and ecophysiology. *Functional Plant Science and Biotechnology*, *1*, 267–287.

Lavaud, J., Six, C., & Campbell, D. A. (2016). Photosystem II repair in marine diatoms with contrasting photophysiologies. *Photosynthesis Research*, *127*(2), 189–199. https://doi.org/10.1007/s11120-015-0172-3

Liefer, J. D., Garg, A., Campbell, D. A., Irwin, A. J., & Finkel, Z. V. (2018). Nitrogen starvation induces distinct photosynthetic responses and recovery dynamics in diatoms and prasinophytes. *PLoS ONE*, *13*(4), 1–24. https://doi.org/10.1371/journal.pone.0195705

Lin, H., Kuzminov, F. I., Park, J., Lee, S. H., Falkowski, P. G., & Gorbunov, M. Y. (2016). Phytoplankton: The fate of photons absorbed by phytoplankton in the global ocean. *Science*, *351*(6270), 264–267. https://doi.org/10.1126/science.aab2213

Lindley, S. T., Bidigare, R. R., & Barber, R. T. (1995). Phytoplankton photosynthesis parameters along 140 degrees W in the equatorial Pacific. *Deep-Sea Research Part II: Topical Studies in Oceanography*, *42*(2–3), 441–463. https://doi.org/10.1016/0967-0645(95)00029-P

Liu, Y., Boss, E., Chase, A., Xi, H., Zhang, X., Röttgers, R., et al. (2019a). Phytoplankton pigment concentration measured by HPLC during POLARSTERN cruises PS93.2, PS99.2 and PS107. *PANGAEA*. https://doi.org/10.1594/PANGAEA.894875

Liu, Y., Boss, E., Chase, A., Xi, H., Zhang, X., Röttgers, R., et al. (2019b). Retrieval of phytoplankton pigments from underway spectrophotometry in the Fram Strait. *Remote Sensing*, *11*(3), 318. https://doi.org/10.3390/rs11030318

Liu, Y., Röttgers, R., Ramírez-Pérez, M., Dinter, T., Steinmetz, F., Nöthig, E. M., et al. (2018). Underway spectrophotometry in the Fram Strait (European Arctic Ocean): a highly resolved chlorophyll a data source for complementing satellite ocean color. *Optics Express*, *26*(14), A678–A696. https://doi.org/10.1364/OE.26.00A678

Locarnini, R. A., Mishonov, A. V., Antonov, J. I., Boyer, T. P., Garcia, H. E., Baranova, O. K., et al. (2010). World Ocean Atlas 2009, volume 1: Temperature, 40 pp. In S. Levitus (Ed.), NOAA Atlas NESDIS 68. Washington, DC: U.S. Government Printing Office 184 pp.

MacIntyre, H. L., Kana, T. M., Anning, J., Geider, R. J., Anning, T., & Geider, R. J. (2002). Photoacclimation of photosynthesis irradiance response curves and photosynthetic pigments in microalgae and cyanobacteria. *Journal of Phycology*, *38*(1), 17–38. https://doi.org/10.1046/j.1529-8817.2002.00094.x

Mackey, M. D., Mackey, D. J., Higgins, H. W., & Wright, S. W. (1996). CHEMTAX - a program for estimating class abundances from chemical markers: Application to HPLC measurements of phytoplankton. *Marine Ecology Progress Series*, *144*, 265–283. https://doi.org/10.3354/meps144265

Magdaong, N. C. M., & Blankenship, R. E. (2018). Photoprotective, excited-state quenching mechanisms in diverse photosynthetic organisms. *The Journal of Biological Chemistry*, *293*(14), 5018–5025. https://doi.org/10.1074/jbc.TM117.000233

Marshall, H. L., Geider, R. J., & Flynn, K. J. (2000). A mechanistic model of photoinhibition. *The New Phytologist*, *145*(2), 347–359. https://doi.org/10.1046/j.1469-8137.2000.00575.x

Masamoto, K., Zsiros, O., & Gombos, Z. (1999). Accumulation of zeaxanthin in cytoplasmic membranes of the cyanobacterium Synechococcus sp. strain PCC7942 grown under high light condition. *Journal of Plant Physiology*, *155*(1), 136–138. https://doi.org/10.1016/S0176-1617(99)80155-2

Megard, R. O., Combs, W. S., Smith, P. D., & Knoll, A. S. (1979). Attenuation of light and daily integral rates of photosynthesis attained by planktonic algae. *Limnology and Oceanography*, *24*(6), 1038–1050. https://doi.org/10.4319/lo.1979.24.6.1038

Mellis, A. (1999). Photosystem-II damage and repair cycle in chloroplasts: What modulates the rate of photodamage in vivo? *Trends in Plant Science*, *4*(4), 130–135. https://doi.org/10.1016/S1360-1385(99)01387-4

Moore, C. M., Suggett, D. J., Hickman, A. E., Kim, Y.-N., Tweddle, J. F., Sharples, J., et al. (2006). Phytoplankton photoacclimation and photoadaptation in response to environmental gradients in a shelf sea. *Limnology and Oceanography*, *51*(2), 936–949. https://doi.org/10.4319/lo.2006.51.2.0936

Müller, P., Li, X. P., & Niyogi, K. K. (2001). Non-photochemical quenching. A response to excess light energy. *Plant Physiology*, *125*(4), 1558–1566. https://doi.org/10.1104/pp.125.4.1558

Nagy, L., Bálint, E., Barber, J., Ringler, A., Cook, K. M., & Maroti, P. (1995). Photoinhibition and law of reciprocity in photosynthetic reactions of Synechocystis sp. PCC 6803. *Journal of Plant Physiology*, *145*(4), 410–415. https://doi.org/10.1016/S0176-1617(11)81763-3

Ni, G., Zimbalatti, G., Murphy, C. D., Barnett, A. B., Arsenault, C. M., Li, G., et al. (2017). Arctic Micromonas uses protein pools and non-photochemical quenching to cope with temperature restrictions on Photosystem II protein turnover. *Photosynthesis Research*, *131*(2), 203–220. https://doi.org/10.1007/s11120-016-0310-6

Oliver, R. L., & Ganf, G. G. (1988). The optical properties of a turbid reservoir and its phytoplankton in relation to photosynthesis and growth (mount bold reservoir, South Australia). *Journal of Plankton Research*, *10*(6), 1155–1177. https://doi.org/10.1093/plankt/10.6.1155

Oliver, R. L., Whittington, J., Lorenz, Z., & Webster, I. T. (2003). The influence of vertical mixing on the photoinhibition of variable chlorophyll a fluorescence and its inclusion in a model of phytoplankton photosynthesis. *Journal of Plankton Research*, *25*(9), 1107–1129. https://doi.org/10.1093/plankt/25.9.1107

Park, Y.-I., Chow, W. S., & Anderson, J. M. (1995). Light inactivation of functional photosystem II in leaves of peas grown in moderate light depends on photon exposure. *Planta*, *196*(3), 401–411. https://doi.org/10.1007/BF00203636

Peloquin, J., Swan, C., Gruber, N., Vogt, M., Claustre, H., Ras, J., et al. (2013). The MAREDAT global database of high performance liquid chromatography marine pigment measurements. *Earth System Science Data*, *5*(1), 109–123. https://doi.org/10.5194/essd-5-109-2013

Porcar-Castell, A., Bäck, J., Juurola, E., & Hari, P. (2006). Dynamics of the energy flow through photosystem II underchanging light conditions: a model approach. *Functional Plant Biology*, *33*, 229–239. https://doi.org/10.1071/FP05133

Polimene, L., Brunet, C., Allen, J. I., Butenschön, M., White, D. A., & Llewellyn, C. A. (2012). Modelling xanthophyll photoprotective activity in phytoplankton. *Journal of Plankton Research*, *34*(3), 196–207. https://doi.org/10.1093/plankt/fbr102

Polimene, L., Brunet, C., Butenschön, M., Martinez-Vicente, V., Widdicombe, C., Torres, R., & Allen, J. I. (2014). Modelling a light-driven phytoplankton succession. *Journal of Plankton Research*, *36*(1), 214–229. https://doi.org/10.1093/plankt/fbt086

R Core Team (2018). *R: A Language and Environment for Statistical Computing*. Vienna, Austria: R Foundation for Statistical Computing.

Raven, J. A., & Crawfurd, K. (2012). Environmental controls on coccolithophore calcification. *Marine Ecology Progress Series*, *470*, 137–166. https://doi.org/10.3354/meps09993

Ross, O. N., Geider, R. J., Berdalet, E., Artigas, M. L., & Piera, J. (2011). Modelling the effect of vertical mixing on bottle incubations for determining in situ phytoplankton dynamics. I. Growth rates. *Marine Ecology Progress Series*, *435*, 13–31. https://doi.org/10.3354/meps09193

Schartau, M., Engel, A., Schröter, J., Thoms, S., Völker, C., & Wolf-Gladrow, D. (2007). Modelling carbon overconsumption and the formation of extracellular particulate organic carbon. *Biogeosciences*, *4*(4), 433–454. https://doi.org/10.5194/bg-4-433-2007

Schlüter, L., Møhlenberg, F., Havskum, H., & Larsen, S. (2000). The use of phytoplankton pigments for identifying and quantifying phytoplankton groups in coastal areas: testing the influence of light and nutrients on pigment/chlorophyll a ratios. *Marine Ecology Progress Series*, *192*, 49–63. https://doi.org/10.3354/meps192049

Schourup-Kristensen, V., Sidorenko, D., Wolf-Gladrow, D. A., & Völker, C. (2014). A skill assessment of the biogeochemical model REcoM2 coupled to the Finite Element Sea Ice – Ocean Model (FESOM1.3). *Geoscientific Model Development*, *7*(6), 2769–2802. https://doi.org/10.5194/gmd-7-2769-2014

Serôdio, J., Schmidt, W., & Frankenbach, S. (2017). A chlorophyll fluorescence-based method for the integrated characterization of the photophysiological response to light stress. *Journal of Experimental Botany*, *68*(5), erw492. https://doi.org/10.1093/jxb/erw492

Six, C., Finkel, Z. V., Irwin, A. J., & Campbell, D. A. (2007). Light variability illuminates niche-partitioning among marine picocyanobacteria. *PLoS ONE*, *2*(12), e1341. https://doi.org/10.1371/journal.pone.0001341

Six, C., Sherrard, R., Lionard, M., Roy, S., & Campbell, D. A. (2009). Photosystem II and pigment dynamics among ecotypes of the green alga Ostreococcus. *Plant Physiology*, *151*(1), 379–390. https://doi.org/10.1104/pp.109.140566

Soppa, M. A., Hirata, T., Silva, B., Dinter, T., Peeken, I., Wiegmann, S., & Bracher, A. (2014). Global retrieval of diatom abundance based on phytoplankton pigments and satellite data. *Remote Sensing*, *6*(10), 10,089–10,106. https://doi.org/10.3390/rs61010089

Stolte, W., Kraay, G. W., Noordeloos, A. A. M., & Riegman, R. (2000). Genetic and physiological variation in pigment composition of Emiliania huxleyi (Prymnesiophyceae) and the potential use of its pigment ratios as a quantitative physiological marker. *Journal of Phycology*, *36*(3), 529–539. https://doi.org/10.1046/j.1529-8817.2000.99158.x

Stow, C. A., Jolliff, J., McGillicuddy, D. J., Doney, S. C., Allen, J. I., Friedrichs, M. A., et al. (2009). Skill assessment for coupled biological/physical models of marine systems. *Journal of Marine Systems*, *76*(1–2), 4–15. https://doi.org/10.1016/j.jmarsys.2008.03.011

Strain, H. H., Manning, W. M., & Hardin, G. (1944). Xanthophylls and carotenes of diatoms, brown algae, dinoflagellates, and sea-anemones. *The Biological Bulletin*, *86*(3), 169–191. https://doi.org/10.2307/1538339

Tagliabue, A., Mtshali, T., Aumont, O., Bowie, A. R., Klunder, M. B., Roychoudhury, A. N., & Swart, S. (2012). A global compilation of dissolved iron measurements: Focus on distributions and processes in the Southern Ocean. *Biogeosciences*, *9*(6), 2333–2349. https://doi.org/10.5194/bg-9-2333-2012

Taylor, B. B., & Bracher, A. (2017). Pigment concentrations measured in surface water during SONNE cruise SO202/2 (TRANSBROM). *PANGAEA*. https://doi.org/10.1594/PANGAEA.880235

Taylor, B. B., Torrecilla, E., Bernhardt, A., Taylor, M. H., Peeken, I., Röttgers, R., et al. (2011a). Bio-optical provinces in the eastern Atlantic Ocean and their biogeographical relevance. *Biogeosciences*, *8*(12), 3609–3629. https://doi.org/10.5194/bg-8-3609-2011

Taylor, B. B., Torrecilla, E., Bernhardt, A., Taylor, M. H., Peeken, I., Röttgers, R., et al. (2011b). Pigments of phytoplankton during POLARSTERN cruise ANT-XXV/1. *PANGAEA*. https://doi.org/10.1594/PANGAEA.819070

Ting, C. S., & Owens, T. C. (1993). Photochemical and nonphotochemical fluorescence quenching processes in the diatom Phaeodacfyhm fricornutum. *Plant Physiology*, *101*(4), 1323–1330. https://doi.org/10.1104/pp.101.4.1323

Trees, C. C., Clark, D. K., Bidigare, R. R., Ondrusek, M. E., & Mueller, J. L. (2000). Accessory pigments versus chlorophyll a concentrations within the euphotic zone: A ubiquitous relationship. *Limnology and Oceanography*, *45*(5), 1130–1143. https://doi.org/10.4319/lo.2000.45.5.1130

Trimborn, S., Hoppe, C. J. M., Taylor, B. B., Bracher, A., & Hassler, C. S. (2015). Physiological characteristics of open ocean and coastal phytoplankton communities of Western Antarctic Peninsula and Drake Passage waters. *Deep Sea Research Part I: Oceanographic Research Papers*, *98*, 115–124. https://doi.org/10.1016/j.dsr.2014.12.010

Uitz, J., Claustre, H., Morel, A., & Hooker, S. B. (2006). Vertical distribution of phytoplankton communities in open ocean: An assessment based on surface chlorophyll. *Journal of Geophysical Research*, *111*, C08005. https://doi.org/10.1029/2005JC003207

Violle, C., Navas, M.-L., Vile, D., Kazakou, E., Fortunel, C., Hummel, I., & Garnier, E. (2007). Let the concept of trait be functional! *Oikos*, *116*(5), 882–892. https://doi.org/10.1111/j.2007.0030-1299.15559.x

Wagner, H., Jakob, T., & Wilhelm, C. (2006). Balancing the energy flow from captured light to biomass under fluctuating light conditions. *The New Phytologist*, *169*(1), 95–108. https://doi.org/10.1111/j.1469-8137.2005.01550.x

Webb, W. L., Newton, M., & Starr, D. (1974). Carbon dioxide exchange of Alnus rubra: a mathematical model. *Oecologia*, *17*(4), 281–291. https://doi.org/10.1007/BF00345747

Westberry, T., Behrenfeld, M. J., Siegel, D. A., & Boss, E. (2008). Carbon-based primary productivity modeling with vertically resolved photoacclimation. *Global Biogeochem Cycles*, *22*, GB2024. https://doi.org/10.1029/2007GB003078

Wilson, A., Ajlani, G., Verbavatz, J.-M., Vass, I., Kerfeld, C. A., & Kirilovsky, D. (2006). A soluble carotenoid protein involved in phycobilisome-related energy dissipation in cyanobacteria. *Plant Cell*, *18*(April), 992–1007. https://doi.org/10.1105/tpc.105.040121.1981

Zindler, C., Bracher, A., Marandino, C. A., Taylor, B. J., Torrecilla, E., Kock, A., & Bange, H. W. (2013). Sulphur compounds, methane, and phytoplankton: Interactions along a north–south transit in the western Pacific Ocean. *Biogeosciences*, *10*(5), 3297–3311. https://doi.org/10.5194/bg-10-3297-2013

Zonneveld, C. (1998). Photoinhibition as affected by photoacclimation in phytoplankton: A model approach. *Journal of Theoretical Biology*, *193*(1), 115–123. https://doi.org/10.1006/jtbi.1998.0688